DESIGN AND STUDY OF AN AEROSTATIC PARTIAL JOURNAL BEARING

by

S. K. SAHA

DEPARTMENT OF MECHANICAL ENGINEERING

INDIAN INSTITUTE OF TECHNOLOGY, KANPUR

AUGUST 1984

DESIGN AND STUDY OF AN AEROSTATIC PARTIAL JOURNAL BEARING

A thesis submitted
in Partial Fulfilment of the Requirements
for the degree of
MASTER OF TECHNOLOGY

by
S. K. SAHA

to the

DEPARTMENT OF MECHANICAL ENGINEERING
INDIAN INSTITUTE OF TECHNOLOGY, KANPUR
AUGUST 1984

ME-1984-M-SAH-DES

DEDICATED

TO MY

ELDEST BROTHER

CERTIFICATE

This is to certify that the thesis entitled, " DESIGN AND STUDY OF AN AEROSTATIC PARTIAL JOURNAL BEARING" submitted by Mr. S.K. Saha for the award of M. Tech. degree is a record of work carried out under our supervision and has not been submitted elsewhere for a degree.

B.N. Banerjee

Dr. B.N. Banerjee
Assistant Professor
Dept. of Mech. Engg.
I.I.T., Kanpur.

A. Ghosh

Dr. A. Ghosh
Professor
Dept. of Mech. Engg.
I.I.T., Kanpur.

ACKNOWLEDGEMENT

It gives me great pleasure to express my gratitude to Dr. A. Ghosh and Dr. B.N. Banerjee for their constant encouragement, invaluable guidance and fruitful discussions throughout this work.

I am grateful to Dr. R. Singh for his invaluable suggestions and discussions in the course of the work.

I wish to express my sincere thanks to Mr. B.P. Bhartia, Mr. R.M. Jha, Mr. V.K. Viswakarma and Mr. Pannalal for their help im fabrication of the experimental set up.

Thanks are also due to a number of friends who have been very helpful in the course of this work including Mr. D.P. Saini for his neat typing, Mr. A. Ganguli for drawing the figures and Mr. Ayodhya Prasad for duplicating.

S.K. SAHA

CONTENTS

LIST OF FIGURES

NOMENCLATURE

α	$[= \frac{h_o}{c}]$ dimensionless film thickness
γ	$[= \frac{C_p}{C_v}]$ ratio of specific heats of gas
ε	$[= \frac{e}{c}]$ eccentricity ratio
ω	angular velocity of the shaft
μ	coefficient of friction
ρ	density ; ρ_a ambient, ρ_s at supply condition
a	$(= \frac{\pi D}{n})$ width of the equivalent slot
b	(= L-2l), fig. 1.1
c	[= bearing radius - shaft radius] radial clearance
d_o	orifice diameter
d_R	pocket diameter
e	$[= \varepsilon c]$ eccentricity, bearing - journal centre distance
h	film thickness
h_o	measured film thickness
h_R	pocket depth
k	$(= \frac{dW}{dh_o})$ bearing stiffness
l	distance of plane of inlet holes from the end of the bearing
m	mass flow of air per orifice

n	number of orifices per row
t	time
A	orifice area
C_D	coefficient of discharge
C_L	$\left[= \frac{W}{LD(P_s-P_a)}\right]$ load coefficient
C_{L_o}	theoretical load coefficient based on axial flow model
C_p	specific heat at constant pressure
C_v	specific heat at constant volume
D	journal diameter
F	friction force
K_g	$\left[= \frac{P_f-P_a}{P_s-P_a}\right]$ gauge pressure ratio
L	length of the bearing
M	total mass flow of air into bearing
M_c	disturbing moment
M'_c	restoring moment
N_T	total number of orifices in the bearing
P_a	atmospheric pressure
P_f	$\left[= \frac{W}{LD}\right]$ average bearing film pressure
P_s	absolute supply pressure
P_1	pressure upstream of the orifice
P_2	pressure downstream of the orifice
Q	total volume flow of air into the bearing

R	gas constant
T_a	atmospheric temperature
T_s	temperature at supply condition
T_f	frictional torque
W	load on the bearing

ABSTRACT

Externally pressurized bearings constitute an important class of load supporting devices, especially under conditions of high load and small relative velocities. Much work has been done to seek an understanding of the mechanics of these bearings, but to date the best results have been obtained by means of numerical solutions. Consequently, no simple procedure exists for designing such bearings. In the present work, an aerostatic partial journal bearing is designed and tested for operating characteristics. From the test data, a procedure for designing such a bearing is suggested which, though only a first formulation based on limited data, has the virtue of being simple. The procedure is based on a simple empirical relation involving the shaft load, supply pressure and film thickness.

CHAPTER - I

INTRODUCTION

1.1 The Aerostatic Bearing

The rapid advances in technology over the last three decades have placed unprecedented demands on machinery and the machine tools which produce the components of these machinery. Tribological design has become more challenging than ever before and, in the realm of bearings alone, fascinating ideas have been proposed and converted to reality. Shaft speeds and loads, operating temperatures, environmental factors and standards of precision have become so exacting that revolutionary changes have occurred in lubrication technology. The aerostatic bearing (" gas bearing") is one of a breed of bearings that have become popular in the past three decades. The load is supported by a film f pressurized air fed in from a compressor or a compressed air cylinder. High loads can be supported even at arbitrarily low speeds, at all temperatures and with no environmental fall out. Such bearings can, besides, have very large stiffness and thus offer great positional accuracy.

1.1.1 Characteristics of the aerostatic bearing

The aerostatic bearing is often called 'externally pressurized' because the pressurized air in the gas film is obtained from an external source, usually a compressor. The gas from the external source is fed into the bearing clearance space through flow restrictors which, in the simplest cases, are just feed holes in the bearing surfaces, and escapes continuously to the atmosphere from the edges of the bearing. It requires power to be expended continuously in maintaining the supply of pressurized gas, and this feature is a major design consideration since excessive gas flow can render the bearing uneconomical.

The mode of operation of an aerostatic journal bearing is explained with reference to the typical full journal bearing (fig. 1.1). The bearing consists of a cylindrical bush into which are drilled rows of gas feed holes spaced evenly around the bearing circumference. Compressed gas from an external source is usually supplied to a manifold or reservoir which supplies the feed holes. From the reservoir the gas flows through the feed holes into the clearance between the shaft and the bush and then axially to the ends of the bearing where it exhausts to the atmosphere. The pressure in the reservoir is the gas supply pressure P_s. The pressure falls as the gas flows

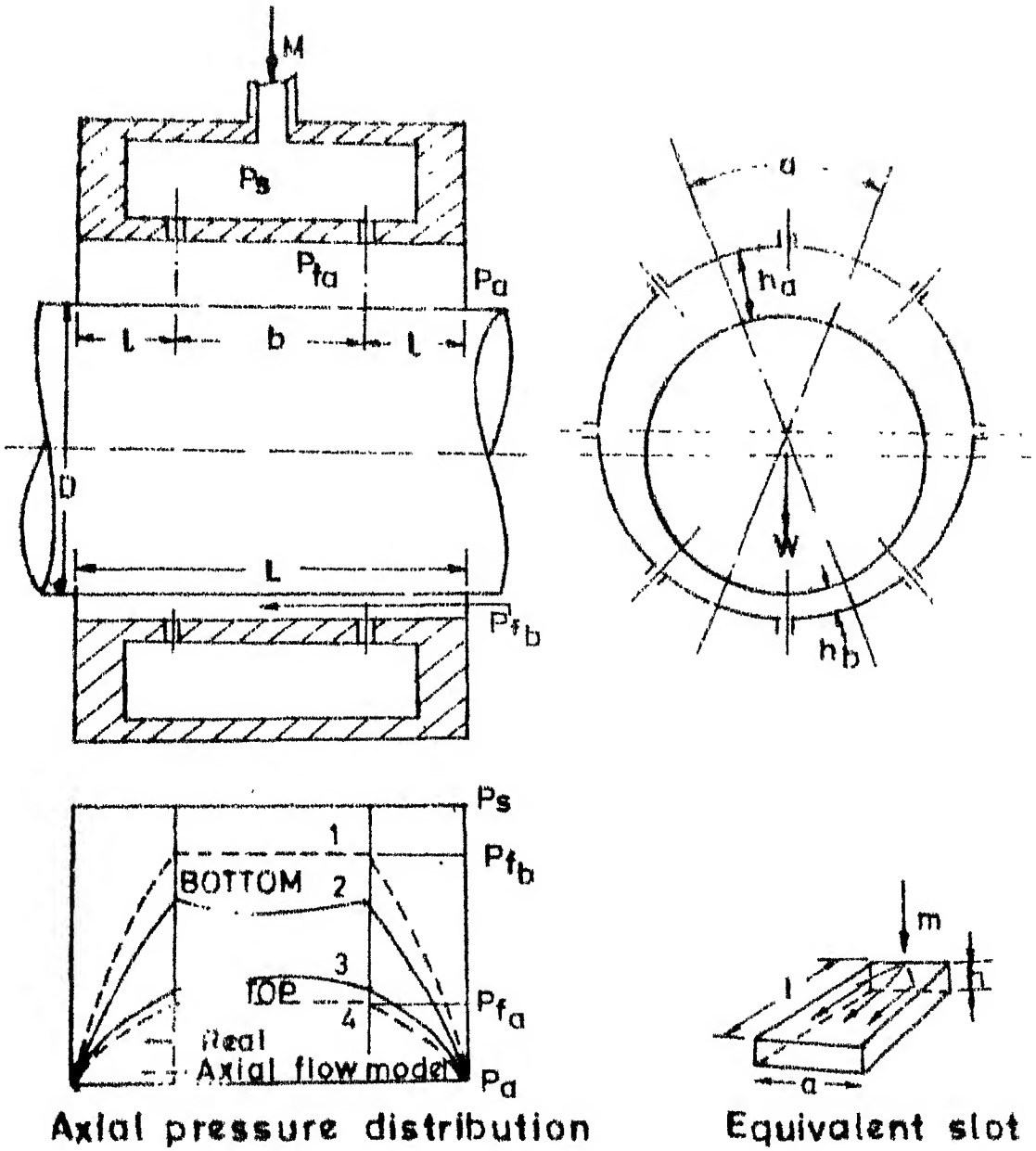

Axial pressure distribution

Equivalent slot

FIG. 1.1 AN EXTERNALLY PRESSURIZED JOURNAL BEARING

through the feed holes and enters the bearing clearance at a pressure P_f , exhausting at the end of the bearing at a pressure P_a (i.e. atmospheric pressure).

With no load applied to the shaft (and neglecting its weight), the shaft adopts a concentric position in the bush. In this case the pressure is reasonably uniform around the bearing circumference and $P_{f_a} = P_{f_b}$.

When a load is applied to the shaft in the vertically downward direction, the shaft is deflected in that direction so that the clearance at the top of the bearing is increased and that at the bottom is reduced. At the top of the bearing the resistance to the flow of gas escaping to the atmosphere is thus reduced so that more gas flows in through the top feed holes. This flow increases the pressure drop through the feed holes and the pressure P_{f_a} falls. Simultaneously, at the bottom of the bearing the resistance to the flow of gas escaping to the atmosphere is increased so that less gas flows through the bottom feed holes. The pressure drop through these feed holes is reduced and the pressure P_{f_b} rises. A difference of pressure now exists across the horizontal diameter of the shaft to balance the applied load.

The viscosity of air is lower, by several orders of magnitude, than that of conventional liquid lubricants

within the same temperature range. For newtonian fluids, the frictional torque is proportional to the viscosity of the lubricant. Thus, frictional losses are substantially reduced in aerostatic bearings. At the same time, the low viscosity does not impair the load capacity which, in an aerostatic bearing, is determined solely by the supply pressure. Also, air is suitable for lubrication at high temperatures when hydrocarbon lubricants may become unstable. At the higher pressures compressibility effects on the pressure profile within the bearing have a significant influence on the performance characteristics, namely, the load carrying capacity, rate of gas consumption and stiffness of the bearing [1].

Multi-pad externally pressurized bearings are self compensating in that, if a disturbance of the operating configuration occurs, a chain of events are set up to restore the operating configuration. This is illustrated by a four-pad thrust bearing (fig. 1.2). In normal operation, the rotating counterface runs parallel to the bearing. If a disturbing moment M_c tilts the counterface, the film thickness over pad 1 decreases while that over pad 3 increases. Consequently, the flow out of pad 1 decreases and that out of pad 3 increases. The pressure drop across the orifice depends on the flow rate. Thus P_f at pad 1 is now more than P_f at pad 3, which sets up a restoring

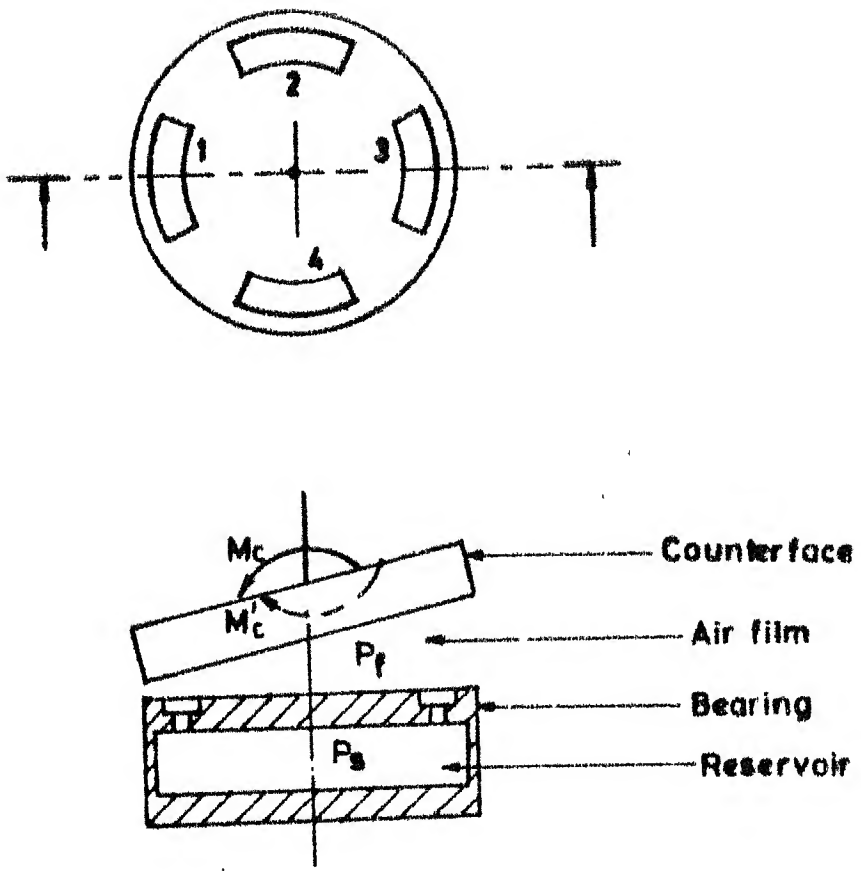

FIG.1.2 THRUST BEARING EXPLAINING COMPENSATION

moment M'_c. Compensation can be achieved by means of flow restrictors of the orifice and capillary types or by ensuring a constant flow rate [2], but these will not be discussed here.

1.1.2 Fields of application

One important field of application of aerostatic bearings is machine tools. The advantages of the application of aerostatic bearings to machine tool spindles result from three properties of aerostatic bearings, namely low friction, precise axis definition and the absence of wear. In comparison with spindles with ball or roller bearings the lower level of vibration of aerostatic bearings is also advantageous. This is particularly so in relation to the generation of precise workpiece geometry and high orders of surface finish, and in ensuring a long life of the cutting tool, drill bit or grinding wheel. Another application includes guide and slide ways of CNC machine tools which takes advantages of the high stiffness, smooth movement, absence of stick-slip and no wear of aerostatic bearings.

The applications of aerostatic bearings to scientific instruments are numerous. One large group of applications, which includes a variety of balances, wind tunnel balances, dynamometers, frictionless pivots and

pulleys, takes advantage of the effectively zero friction of aerostatic bearings at zero speed to eliminate the effects of 'stiction' which is often a problem in instrument bearings.

Aerostatic bearings are also used in turbine flowmeters for gases and in some medical equipment like high speed air turbine dental drills.

The natural applications of the aerostatic bearing are in the situations where relative motion occurs at very low speeds and where the use of a lubricating oil would entail an intolerable pollution of the system environment.

1.1.3 Advantages and disadvantages

The advantages offered by externally pressurized air bearings include :

i) Stable operation

ii) High load capacity

iii) No contamination of the environment and therefore no need of sealing

iv) Low friction

v) Absence of wear and long life

vi) Effectiveness under extreme temperature conditions- hot or cold

vii) Precise position control

viii) Low vibration and noise level

The principal disadvantage is the dependence on a continuous supply of air from an external source and, in some cases, the high compressor power required and the capital cost of the air supply system.

1.2 Brief Outlines of Previous Work

The basic aspects of gas bearing technology was understood by 1959. The gas lubricating film equations had been established analytically and confirmed experimentally. Successful gas bearings had been designed for several applications, including gyros, supports for magnetic heads in disk files for computers, and special machine tools. Though fairly successful, the bearings were usually far from optimum and applications were still at the exploratory stage.

1.2.1 The axial flow model

Shires [3] gave a good description of design technique for externally pressurized bearings. It was felt that the theoretical flow pattern in the clearance of a pressurized journal bearing is complicated by circumferential components and by interactions between jets. However, for bearings which are short in relation to

their diameter and which have circumferential recesses at the feed holes, the flow from the row of feed holes to the ends is almost axial, and a simple theoretical treatment is possible. For other bearing geometries a correction for length and the number and type of inlets may be applied.

Robinson and Sterry [4] used this type of axial flow model. The following is a summary of the relationships used, and an indication of the significance of the parameters in design.

The mathematical model represents the continuously varying clearance space by discrete rectangular slots, each corresponding to one of the feed holes in a row. Fig. 1.1 shows an equivalent slot. The width of the slot is

$$a = \frac{\pi D}{n}$$

where D is the bearing diameter and n the number of feed holes in the row. The length of the slot is l (ref. fig. 1.1). For the space b between rows, the model assumes a constant pressure P_f which is the same as the pressure at the inner end of the slot. Thus each slot is said to be extended over a constant pressure region of length b/2. The depth of the slot is the local clearance.

The gas force on the shaft can be determined [3] by first obtaining the pressure in each slot and its extension

and then integrating over all the slots. The load capacity of the bearing can thus be obtained in terms of the bearing dimensions, gas properties, supply pressure and eccentricity.

The general expression for load coefficient calculated in this way is given by Robinson [4] for an even number of feed holes as

$$C_L = 2 \sin \frac{\pi}{n} \left(1 - \frac{2l}{3L}\right) \left[(K_g)_1 \cos \frac{\pi}{n} + (K_g)_2 \cos \frac{3\pi}{n} + \ldots (K_g)_{\frac{n}{2}} \cos \left(\pi - \frac{\pi}{n}\right)\right] \quad \ldots \quad (1.1)$$

where, $$C_L = \frac{W}{L\ D\ (P_s - P_a)} \quad (1.2)$$

is the load coefficient and

$$K_g = \frac{P_f - P_a}{P_s - P_a} \quad (1.3)$$

is the slot pressure factor and the subscripts of K_g indicate the location of the feed hole and hence the clearance for which K_g is calculated.

1.2.2 The influence of circumferential flow

The axial flow model so far described gives values of load coefficient which can not be attained in practice. In actual bearings there is a peripheral leakage of gas from the high pressure side to the low pressure

side which reduces their load capacity appreciably. Pictures of the complex flow patterns have been obtained by introducing small quantities of oil with the gas and afterwards blowing a powder over the surfaces [5].

A theoretical treatment applicable to small eccentricities has been presented by Pinkus and Sternlicht [6], but unfortunately the solution is only for a bearing with a single central row of feed holes. Because of its limitations to small eccentricities this theory tends to underestimate the effect of the circumferential flow and overestimate the maximum load capacity (which corresponds to an eccentricity ratio of 1).

A simplified theoretical treatment has been developed by Shires [7] the solution of which contains an empirical term for the equivalent length of the circumferential leakage path. Using a comprehensive series of experimental results obtained by Robinson [4] an empirical value of this constant was derived to give the final solution in the following form :

$$\frac{C_L}{C_{L_o}} = 0.315 \cdot \frac{\left[\frac{\cosh(6.36\ l/D)-1}{\sinh(6.36\ l/D)} + \tanh\left(6.36\ \frac{L-2l}{D}\right)\right]}{\left[\ \frac{L-l}{D}\ \right]} \qquad \ldots \quad (1.4)$$

where C_{L_o} is the theoretical load coefficient based on

the axial flow model and C_L is the actual load coefficient including the effects of circumferential flow.

Lemon [8] has given an analysis for calculating the characteristics, such as stiffness, flow, and load of an externally pressurized gas journal bearing. The analysis was obtained through a standard one-dimensional flow approach modified to take into account the effect of circumferential pressure variations. The assumed pressure distribution was verified experimentally. A major shortcoming of this analysis is that the form of this circumferential pressure distribution is not a function of the length to diameter ratio. For very long bearings the circumferential pressure drop between the gas inlets will be somewhat greater than that he has assumed, while for short bearings it will be somewhat less. From this analysis, it was revealed that the bearing stiffness has an optimum which can be attained by a proper selection of design parameters, such as radial clearance, upstream resistor geometry and supply pressure. This is shown in fig. 1.3.

The detailed effects of circumferential flow on pressure distribution in a bearing with a single row of feed holes have been reported by Powell, Moye and Dwight [9]. They show that on the low clearance side of a loaded bearing the actual value of P_f is much less than the

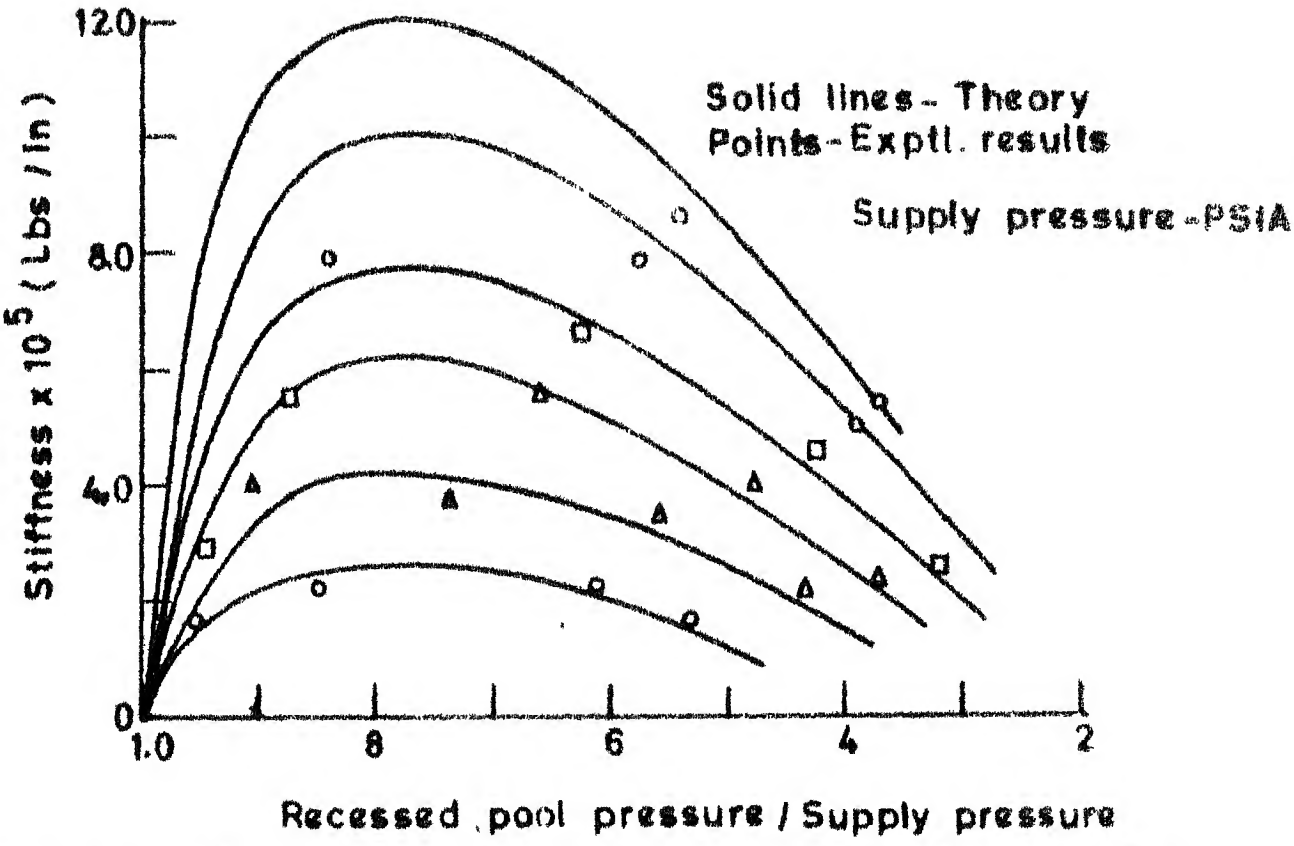

FIG. 1.3 OPTIMISED STIFFNESS AT A PRESSURE RATIO OF APPROX. 0.7 [8]

theoretical value, while on the high clearance side P_f is higher than the theoretical value (curves 2 and 3 of fig. 1.1). In the former case there is a circumferential outflow, so that the purely axial flow model underestimates the net outflow from this region. Likewise, the purely axial flow model overestimates the net outflow from the latter region, where there is a circumferential inflow.

Mazumder [10] did theoretical and experimental studies of externally pressurized gas bearings with multiple supply holes. The method involved a numerical solution by iteration using a digital computer. The solution was obtained for finite journal bearings considering both axial and circumferential flow components. The results obtained from the theory were verified experimentally.

1.3 Objective and Scope of the Present Work

The primary objectives were the design and successful fabrication of a partial aerostatic bearing. A secondary objective was to study some characteristics of the bearing, such as its load capacity, stiffness, film thickness and supply pressure as functions of one another. The other important parameter, viz the mass flow rate of air, could not be studied for want of a suitable flow meter. The objectives did not include any theoretical study.

CHAPTER - 2

DESIGN AND FABRICATION OF A PARTIAL AEROSTATIC BEARING

2.1 Choice of Design Parameters

In view of the discussion of the article 1.1.1, the important parameters in the operation of an aerostatic journal bearing are the film thickness, air flow rate and supply pressure. In addition, the overall size of the bearing, the number and disposition of the compressed air inlets and the geometry of these inlets must be chosen with the application in mind. The shaft diameter and the load on the bearing are usually known a priori.

The available manufacturing facilities may place restrictions on the choice of the type of air inlets to be used as well as on the dimensions of these inlets. The minimum air gap between the shaft and the bearing surface may also be limited by similar restrictions. The air flow rate and the supply pressure, likewise, may be influenced by the capacity of an already existing compressor. For a given load, the average pressure in the bearing gap has a fixed value and the supply pressure is higher for higher flow rates. The air flow rate, in turn,

is higher for larger values of the mean film thickness. Thus operation at the minimum permissible average film thickness minimizes the demands on the compressor in terms of flow rate as well as supply pressure.

The stiffness of the air film is an important consideration when the load is unsteady either in magnitude or in direction. The stiffness depends on the film thickness; for thrust bearings it increases monotonically with decreasing film thickness. When the load direction is steady, partial journal bearings are convenient. For such bearings, the stiffness-film thickness relation is probably similar to that for thrust bearings. Thus minimizing the film thickness amounts to maximizing the stiffness.

Finally, one has to consider the frictional torque on the bearing. One of the primary objectives of designing a bearing is to minimize this torque. Available data indicate that minimizing the film thickness leads to maximization of the frictional torque. One might seek an optimal design that gives the best balance between the compressor power and the power dissipated through friction in the bearing. In general, however, the friction in an aerostatic bearing is so small that one can live with the higher range of frictional torques.

As a starting point in the design of an aerostatic journal bearing, Stout et al [11] recommend the following

- overall bearing length to diameter ratio L/D = 1.0 to 1.5
- ratio of the axial flow land width to bearing length l/L = 0.25
- diametral clearance to diameter ratio 2c/D = 0.5 to 1.5×10^{-3}
- supply pressure in the range of 4 to 6 atmospheres.

The precise values of the above parameters are dependent on the space availability, load and stiffness requirements and mass flow rate, in addition to considerations of ease of manufacture. Stout's recommendations are for full journal bearings.

2.1.1 Choice of number of inlet rows

Aerostatic journal bearings normally have two rows of inlets placed circumferentially around the bearing. The location of these inlets is most often at l/L = 0.25. An alternative arrangement is the single row entry bearing, but the single bearing of this type has no tilt stiffness and no tilt compensation. Keeping this in mind, the double admission bearing configuration was chosen.

2.1.2 Choice of the type of entry

There are normally two kinds of aerostatic journal bearings. They differ in the geometry of the inlet, namely slots and orifices. These types are shown in fig. 2.1. The choice between the two is governed by operational and manufacturing considerations. When the operating eccentricity is low and does not exceed half the radial clearance, both bearing types can be considered approximately equal in load capacity, flow rate and stiffness. This has been experimentally confirmed by Stout et al [11].

The orifice type of inlet was chosen because this is more easily manufactured, the air being admitted to the bearing clearance through straight drilled holes.

2.1.3 Choice of other parameters

Other parameters were chosen as follows

- load - 350 N
- supply pressure P_s of 4 atmospheres
- mean radial clearance of 40 μm
- number of orifices in a row - 5

The shaft diameter was chosen to be 60 mm so as to have reasonably large bearings and hence managable sizes for the air inlet connections.

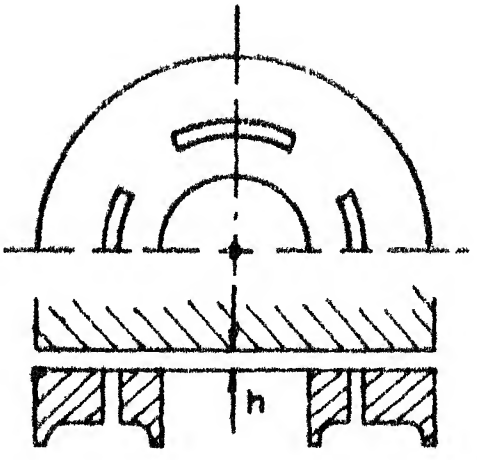

a) Annular thrust bearing with circular inlet slots

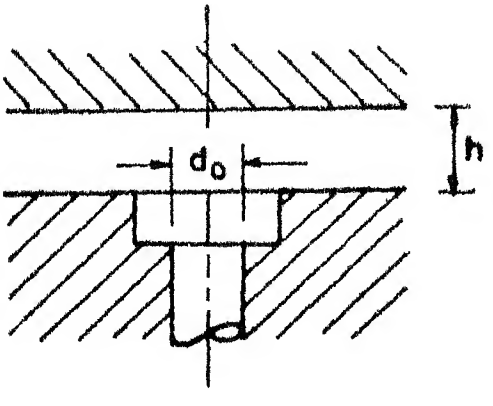

b) Simple orifice inlet

FIG. 2.1

2.2 Design Procedure

Stout et al [11] have given useful design charts and procedures to assist the engineer in designing aerostatic journal bearings and the present bearing has been designed with the help of these charts. The design procedure allows the selection of load capacity, stiffness, flow rate, supply pressure and appropriate bearing dimensions. Fig. 2.2 relates the bearing dimensions, supply pressure, bearing clearance, load capacity and stiffness and can be used in a variety of ways, depending on which criteria are constrained by the particular application. In a similar manner fig. 2.3 deals with the mass flow rate.

Fig. 2.4 affords the evaluation of the most suitable orifice diameter based on the standard design parameters, while fig. 2.5 finds the minimum feeder-hole diameter for a given number of orifices. Fig. 2.6 enables the selection of pocket depth and diameter to avoid pneumatic - hammer instabilities. This characteristic is the result of a time lag between variations in the film pressure and pocket-volume pressure, and can be avoided by minimizing the pocket volume [11].

The following procedure has been followed to use the design charts:

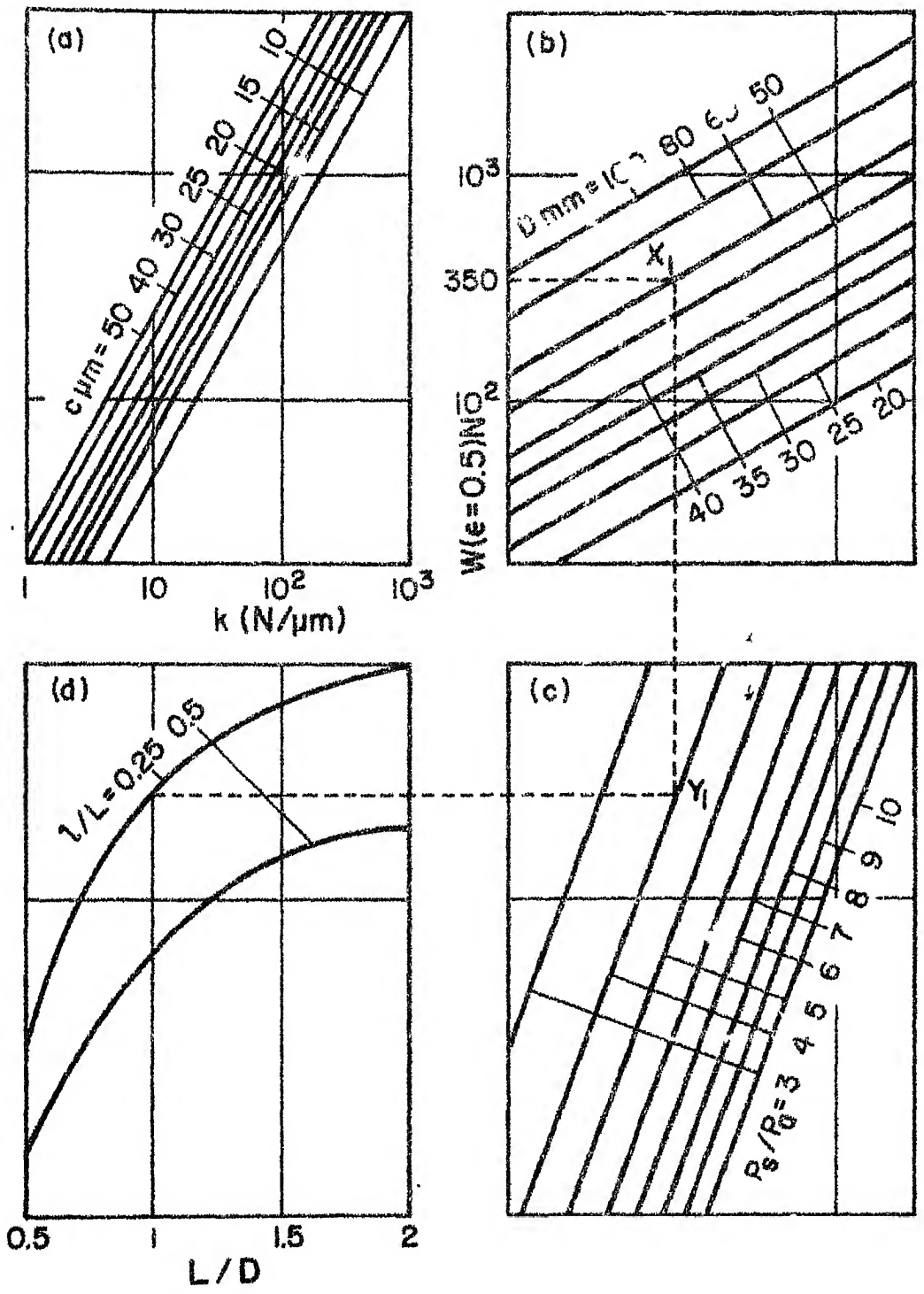

Fig. 2.2 Design chart relating load carrying capacity, bearing dimension and supply pressure [11]

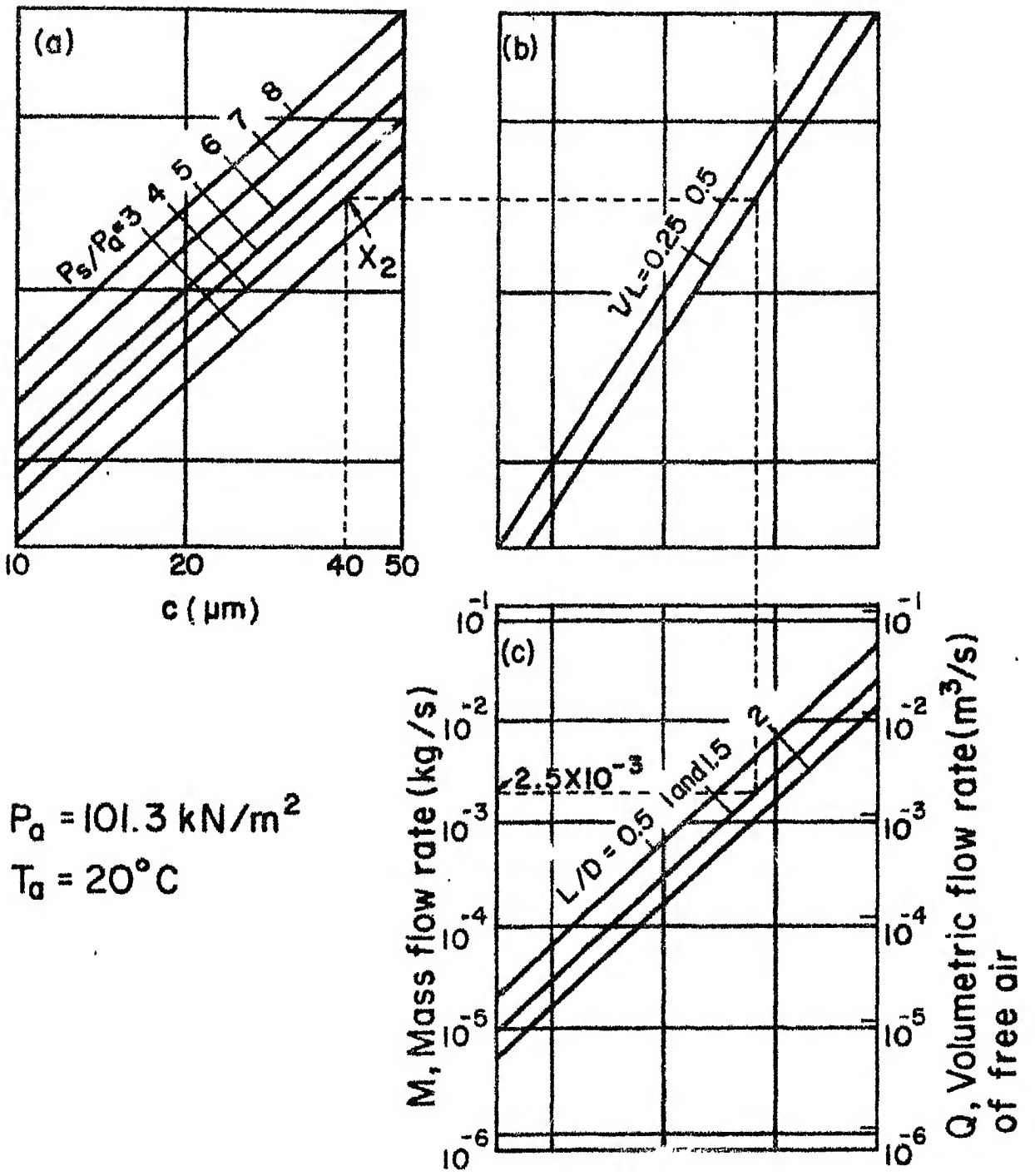

$P_a = 101.3\ kN/m^2$

$T_a = 20°C$

Fig. 2.3 Design chart relating flow rate, clearance and supply pressure [11]

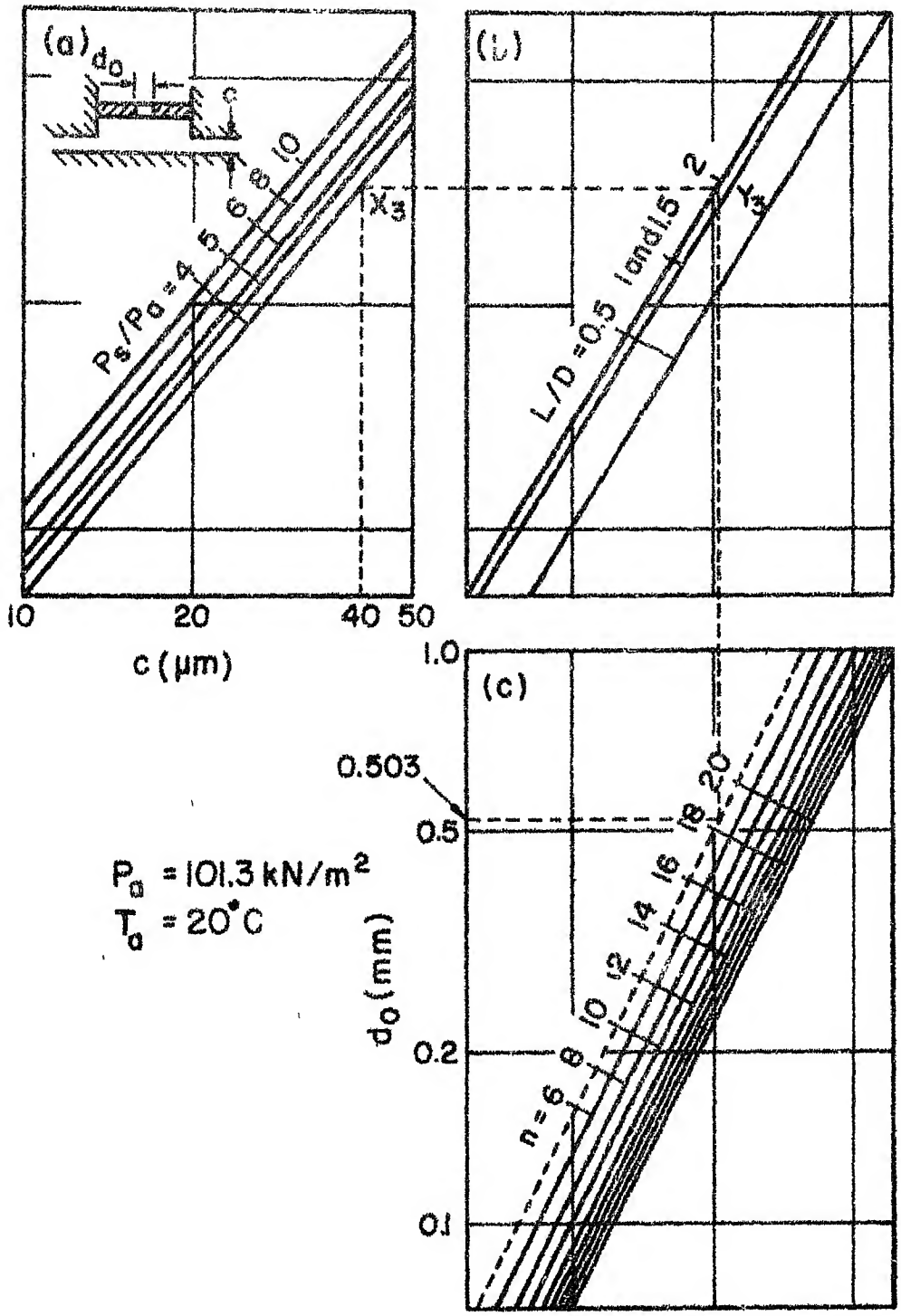

Fig.2.4 Optimum pocketed orifice diameter [11]

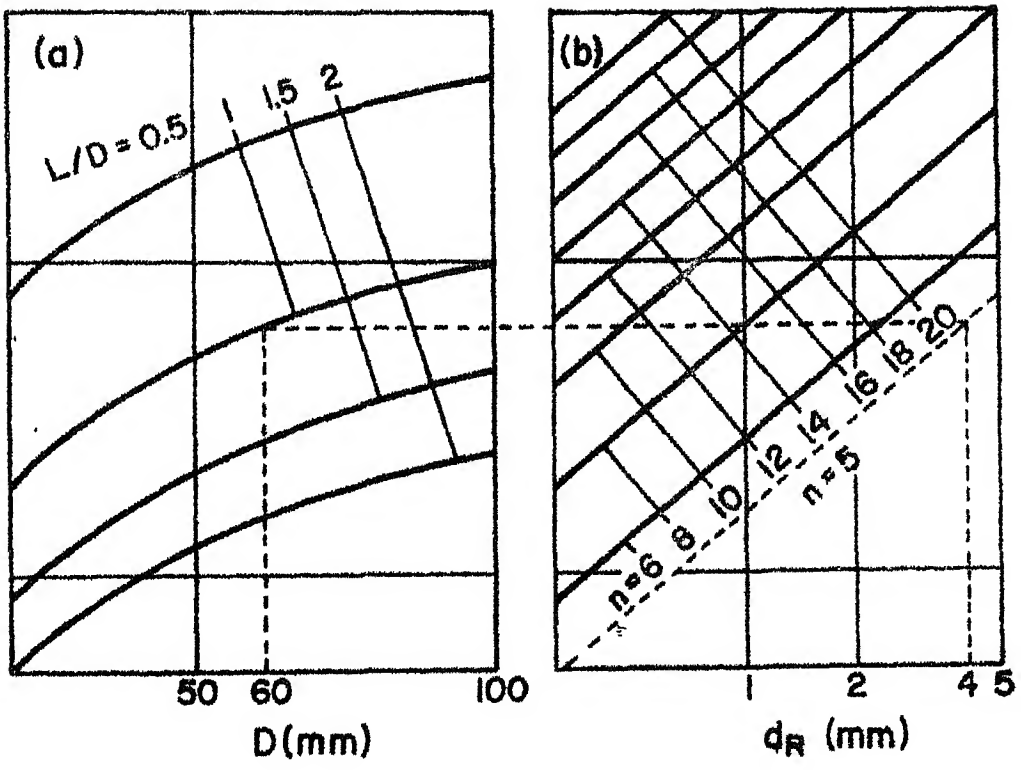

Fig. 2.5 Minimum feeder hole diameter [11]

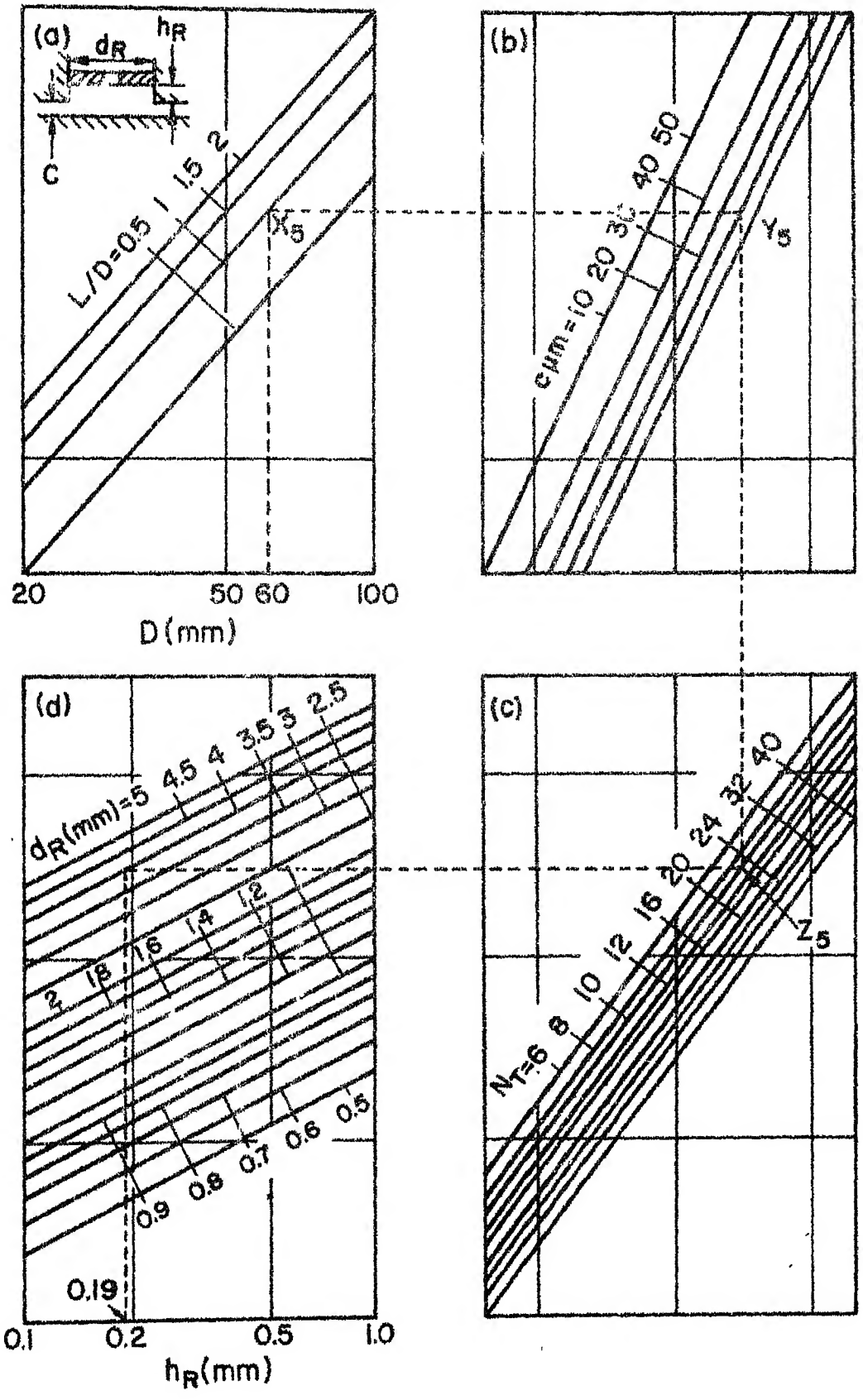

Fig.2.6 Minimum pocket depth to avoid instabilities [11]

i) Enter fig. 2.2(b) at the chosen W = 350 N. The journal diameter D is chosen as 60 mm. This locates a point X_1 on fig. 2.2(b).

ii) From X_1 in fig. 2.2(b), drop a vertical to $P_s/P_a = 4$ and this locates a point Y_1 in fig. 2.2(c).

iii) From Y_1 in fig. 2.2(c), draw a horizontal line to intersect the curve $1/L = 0.25$ of fig. 2.2(d). The abscissa of this intersection point gives the value of L/D.

iv) Enter fig. 2.3(a) at the chosen value of c (40 μm) and $P_s/P_a = 4$. This locates a point X_2 in fig. 2.3(a).

v) From X_2 , draw a horizontal line to intersect the line $1/L = 0.25$ of fig. 2.3(b).

vi) Drop vertically from this intersection point to intersect the line L/D = 1 of fig. 2.3(c). The ordinate of this point in fig. 2.3(c) gives the value of the mass flow rate.

vii) Enter fig. 2.4(a) at the chosen value of clearance c (40 μm) and $P_s/P_a = 4$, i.e. at the point X_3.

viii) Draw a horizontal line from X_3 to fig. 2.4(b) to obtain the intersection Y_3 with the line for L/D = 1.

ix) From Y_3 , drop a vertical line to fig. 2.4(c) to intersect the line (extrapolated) for n = 5. An odd number of orifices is chosen so as to have symmetry in the partial journal bearing being designed. The ordinate of this intersection gives the orifice diameter d_o.

x) Enter fig. 2.5(a) at the point X_4 which corresponds to L/D = 1 and the chosen shaft diameter D = 60 mm.

xi) From X_4 , proceed horizontally to fig. 2.5(b) to intersect the line (extrapolated) for n = 5. The abscissa of this intersection gives the value of the recess diameter d_R. It is suggested [11] that d_R should be greater than or equal to $d_o^2/2c$.

xii) Enter fig. 2.6(a) at the chosen value D = 60 mm and the designed value L/D = 1, i.e. at the point X_5.

xiii) Draw a horizontal line from X_5 to fig. 2.6(b) to intersect the line c = 40 μm at the point Y_5.

xiv) Drop vertically from Y_5 to fig. 2.6(c) to obtain the point Z_5 which corresponds to N_T = 10 for the total number of orifices in the two rows.

xv) Go horizontally from Z_5 to fig. 2.6(d) to intersect the line for the designed recess diameter d_R = 4 mm. The abscissa of this intersection gives the recess depth h_R.

The above fifteen steps complete the design. Table 2.1 lists all the dimensions and parameters for the present bearing at the design condition.

2.3 Fabrication

The production of aerostatic bearings requires a high degree of precision and control. An apparently marginal improvement in the precision of the dimensions can result in significant improvements in bearing performance. The experimental set up required one pair of half journal bearings and twenty air inlet plugs to be fabricated.

2.3.1 Bearing bush

The standard brass which contains 70 percent Copper and 30 percent Zinc, has been used for the bearing bush material. The brasses combine a degree of strength, ductility and corrosion resistance at moderate cost. They are easily machined and easily soldered or brazed so that the pressure - tight attachment of the numerous inlet plugs is a relatively simple matter. Brass is also a fairly good bearing material.

To start with a hollow cylinder was cast. While casting, shrinkage allowances and machining allowances were provided to the inner diameter, outer diameter and

TABLE 2.1

DESIGN DATA FOR THE PRESENT BEARING

Orifice Inlet Type

Chosen values	$W = 350$ N
	$D = 60$ mm
	$P_s/P_a = 4$
	$l/L = 0.25$
	$c = 40$ μm
	$n = 5$
Designed values	$L/D = 1$
	$M = 2.5 \times 10^{-3}$ kg/s
	$d_o = 0.503$ mm
	$d_R = 4$ mm
	$h_R = 0.19$ mm

bearing length. Then the cast cylinder was turned, bored and faced in a lathe to give the exact bearing diameter and length. Care has been taken, while boring, to get a good surface finish. Twenty evenly spaced holes of four millimeter diameter were drilled all around the circumference in two rows (ten holes per row) for inserting the air inlet plugs. The drill used was of 3.9 mm diameter. The holes were reamed to 4 mm. diameter to obtain a smooth finish because the inner ends of the holes would be the surfaces of the air pockets. The full cylindrical piece was then cut into two halves through a diametral plane. These two halves were used for the two half journal bearings.

2.3.2 Air inlet plugs

The air inlet plugs are simply the nipples to which the inlet tubes are attached. They are called plugs here because they serve another, and very important, function, viz. the setting of the pocket or recess depth h_R. These plugs can be seen in fig. 2.7. They are made of brass. First the holes of 2 mm diameter were drilled to a depth of 12 mm. The orifices of diameter 0.5 mm were then drilled from the other end. The shoulder that sits on the outside of the bearing bush was machined at a distance of $(15 - h_R)$ mm from the orifice end. When

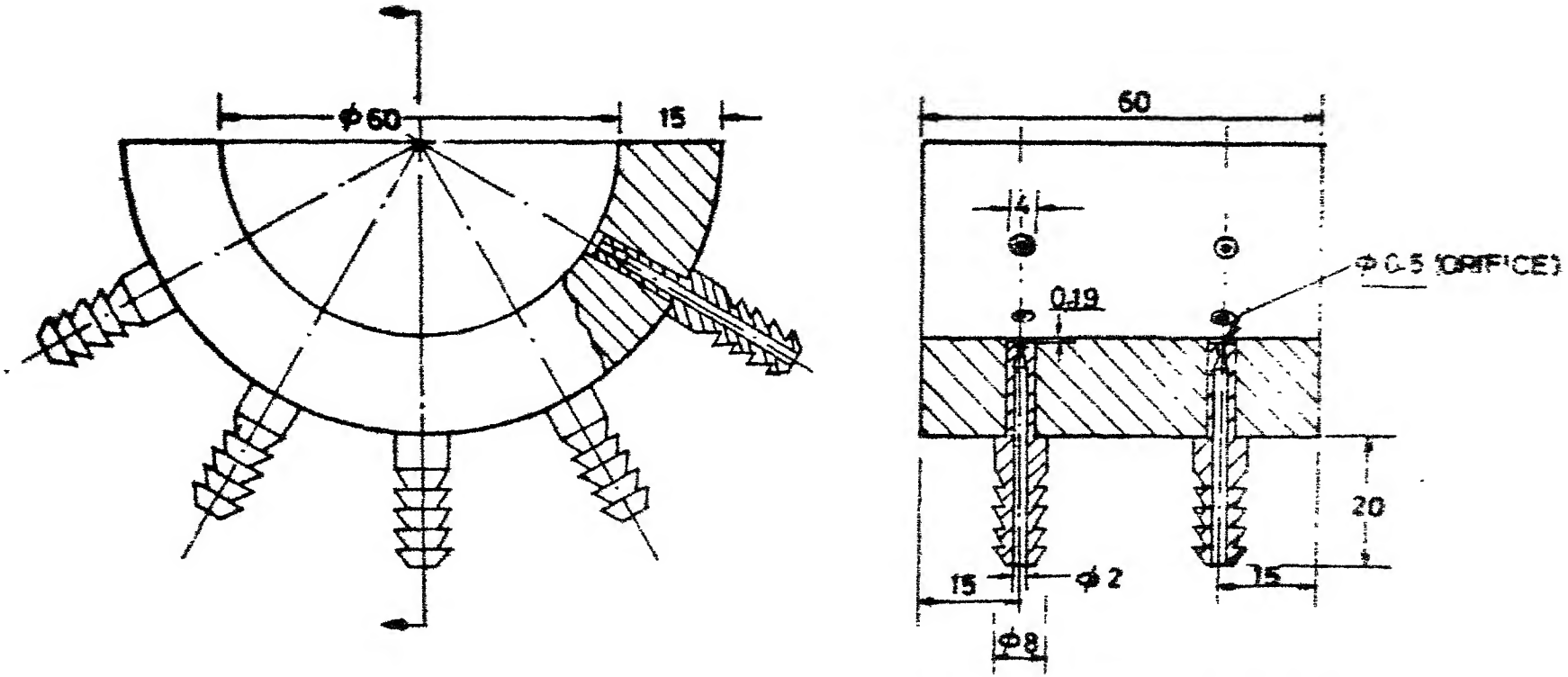

FIG. 2.7 DESIGNED HALF AEROSTATIC JOURNAL BEARING.

the inlet plug was inserted into its socket in the bearing bush, a recess (pocket) of depth h_R = 0.19 mm was autometically obtained. The plug was a mild push fit in its socket. To ensure a leak-proof joint, the plug was brazed onto the bearing bush.

CHAPTER - 3

EXPERIMENTAL SET UP AND TEST RESULTS

3.1 Experimental Set Up

The schematic diagram of the experimental set up is shown in fig. 3.1. The set up consists of the following parts:

i) Shaft

ii) Two aerostatic half journal bearings

iii) Bearing supports

iv) Loading arrangement

v) Dial indicators

vi) Compressed air manifold

vii) Pressure regulator

viii) Air compressor with reservoir.

The compressed air stored in a large reservoir, is passed through the pressure regulator to the manifold. The pressure regulator controls the bearing supply pressure. The manifold supplies air to both the bearings. For static tests, the shaft is loaded by hanging weights at the mid-length of the shaft and the corresponding

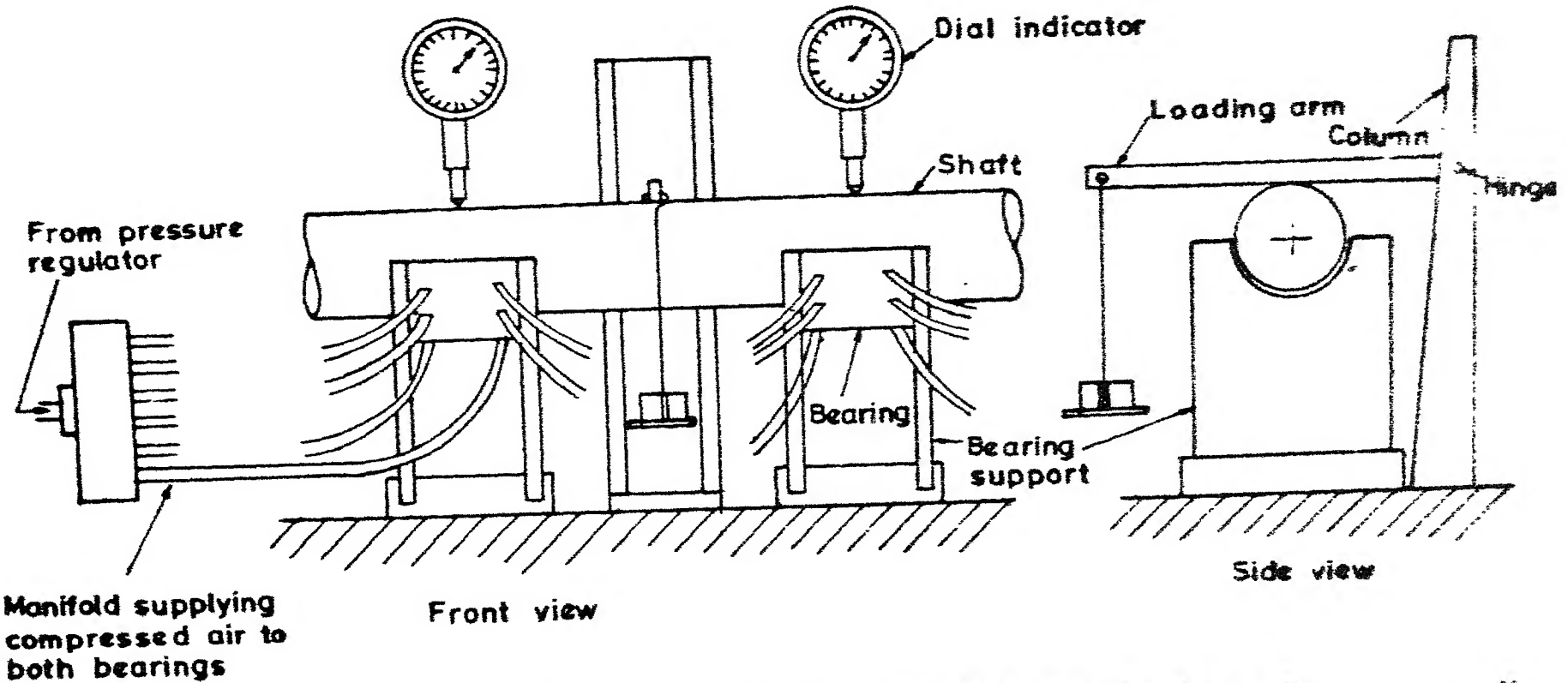

FIG. 3.1 SCHEMATIC DIAGRAM OF THE EXPTL. SET UP

deflection of the shaft in the bearing film is measured by dial indicators located on both bearings. The dial indicator can read a deflection of one micron.

The shaft is made of mild steel and has a cylindrically ground surface which is cleaned thoroughly before being placed on the bearings. The bearings themselves are very carefully aligned.

The loading is done via a lever arm of rectangular cross section which rests on the shaft at its mid-length. One end of this arm is hinged to a column and the loading pan is hung from the other end. It is to be noted that this arrangement does not permit rotation of the shaft under load.

The dial indicator is placed vertically, the stylus of the indicator touching the topmost point on the surface of the journal. The indicator is clamped to a magnetic stand.

Each bearing has a total of ten air inlets in two rows and the manifold supplies air to all these inlets. The manifold consists of twenty polythene tubes emerging from a closed hollow cylinder made of mild steel. Specifications of some of the elements of the set up are given in Appendix-I.

3.2 Test Procedure

Tests were carried out to measure the film thickness at different supply pressures and different loads. The shaft was placed on the two partial journal bearings such that the overhung lengths at the two ends were the same. This was done to ensure that equal loads were carried by the two bearings. The dial indicator was now placed on the journal surface. The top surface of the journal was found by moving the indicator across the shaft and the maximum height could be read from the indicator. The loading arm was placed on the shaft and the weights were kept on the loading pan. With a particular load applied on the bearing, the supply pressure was varied by adjusting the pressure regulator. The supply pressure was gradually increased from zero psig to a maximum pressure of 60 psig and then gradually decreased from 60 psig to zero psig. The dial indicator readings were noted for such cycles of increasing and decreasing pressure. The experiments were repeated several times to check the repeatability of the results. The same experiment was done with different loads applied on the bearing. This was purely a static test and the shaft was not given any rotation.

3.3 Test Results and Discussions

In fig. 3.3 are seen plots of the variation of the film thickness with changes in the supply pressure for different values of the load. This figure shows that as the supply pressure increases, the film thickness also increases for a particular load. This is in accordance with expectation and is explained as follows. The higher supply pressure tends to create a larger upthrust on the shaft, which then rises until the average pressure in the film is just sufficient to support the shaft load. The average film pressure P_f is constant for a given load. As a consequence of the combined effect of the increased film thickness h_o and the increased pressure drop (P_s-P_f) across the orifice, the volume rate of flow of the air also increases. Conversely, a higher volume rate of flow corresponds to a higher pressure drop across the orifice.

The effect of increasing the load is to increase the average film pressure P_f. Thus fig. 3.3 confirms that, for a given film thickness, the supply pressure increases as the load increases.

The variation of load with film thickness for given pressure ratios P_s/P_a is shown in fig. 3.4. These curves are derived from the curves of fig. 3.3. As expected, the film thickness decreases when the load

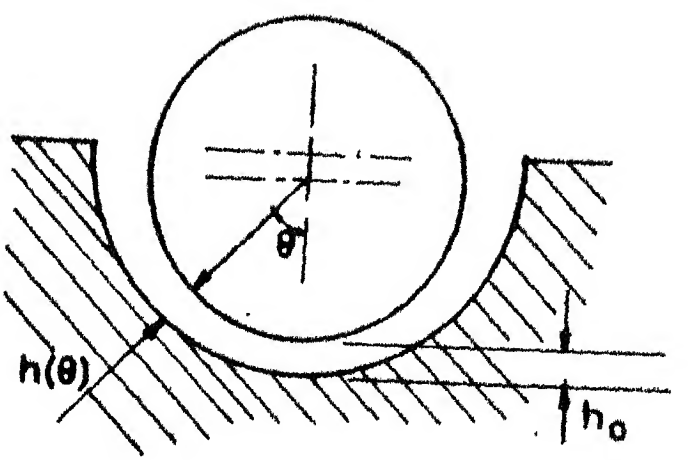

FIG. 3.2 DEFINITION OF FILM THICKNESS h_o

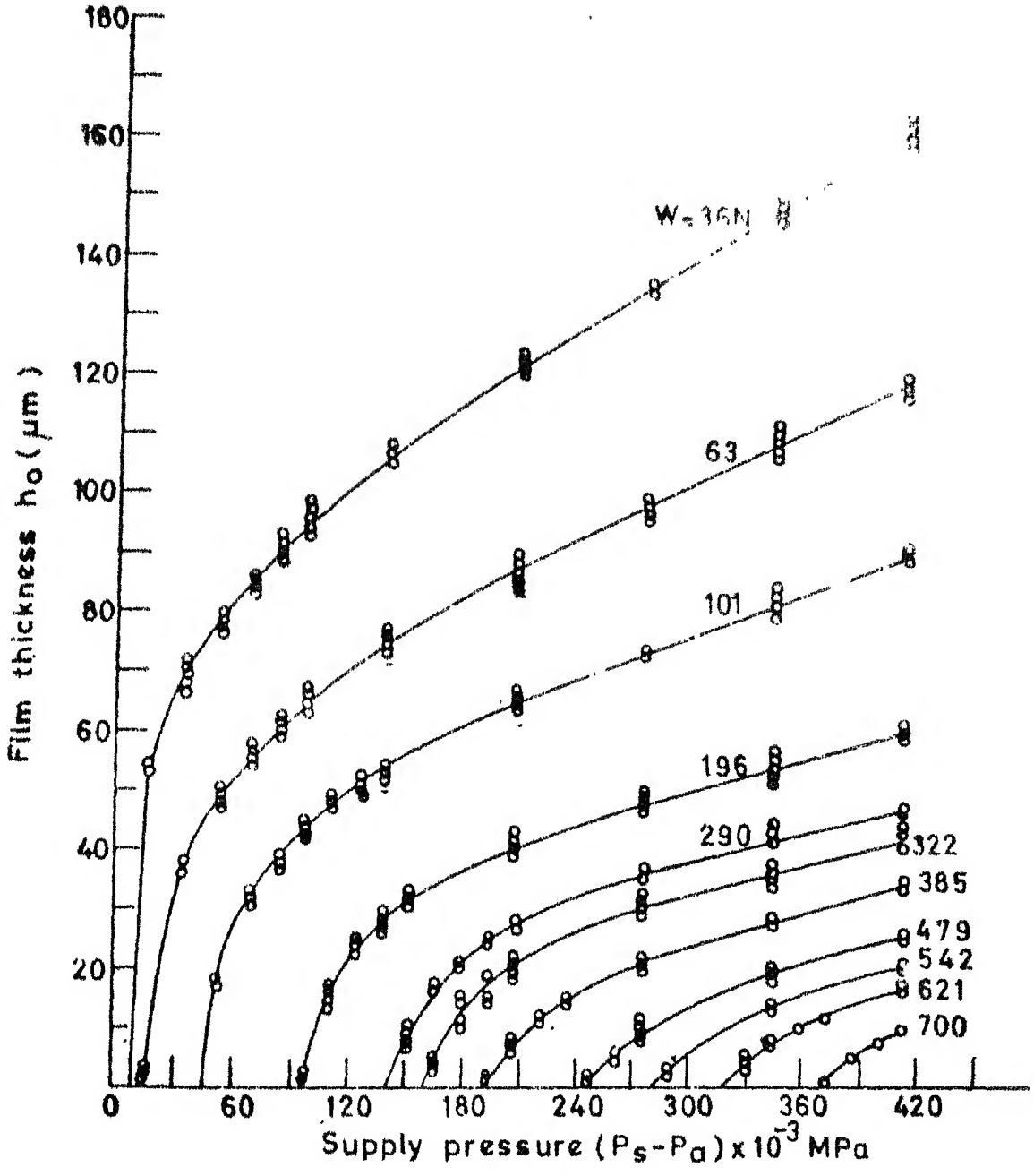

FIG. 3.3 GRAPH OE FILM THICKNESS VS. SUPPLY PRESSURE
(Data points show the experimental results)

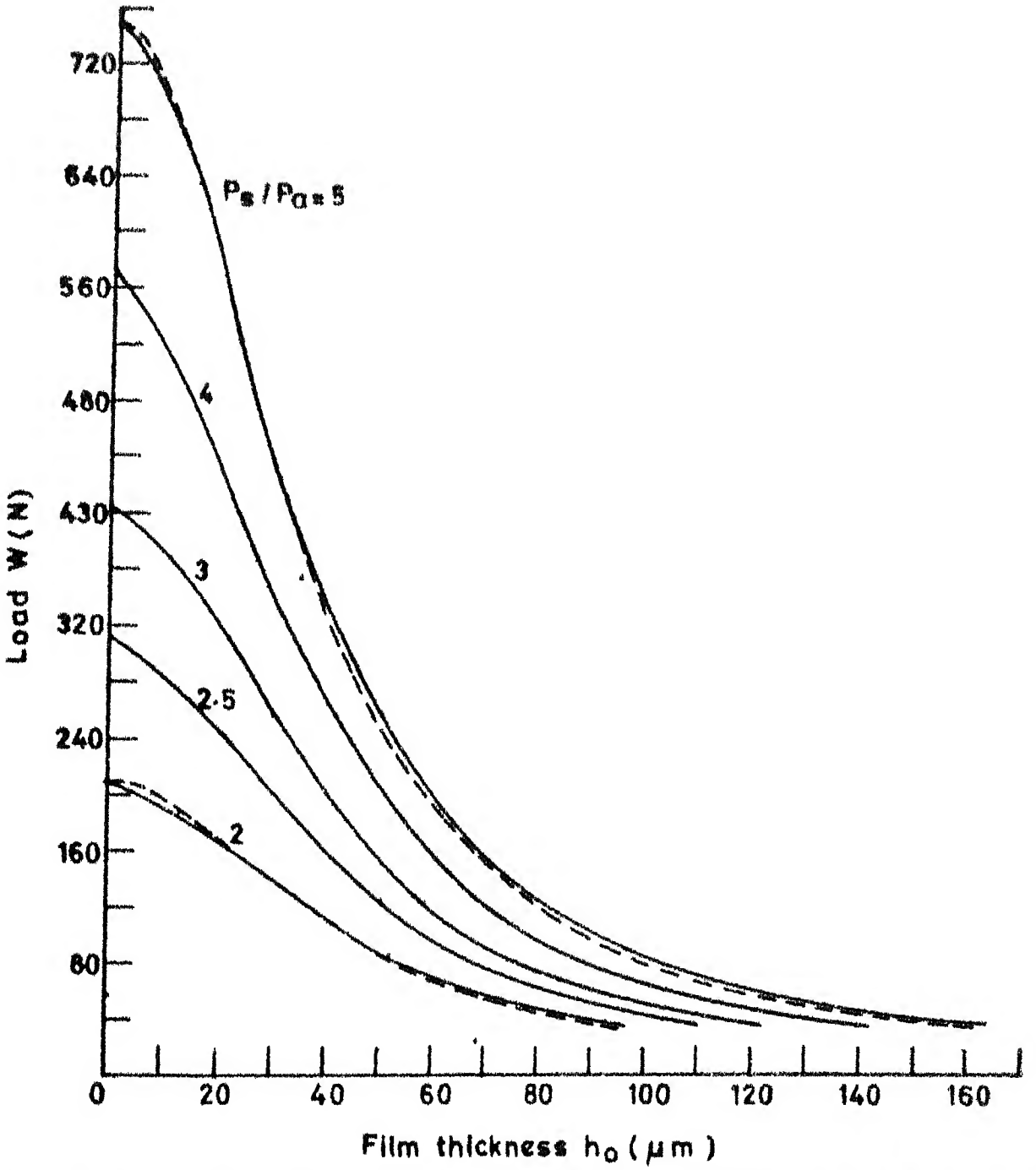

FIG. 3.4 GRAPH OF LOAD Vs. FILM THICKNESS (The solid lines are obtained from fig. 3.3, The two dashed lines are typical of equation 3.1)

increases. The interesting aspect of fig. 3.4 is that each curve indicates the variation of the stiffness of the bearing with changing film thickness. The stiffness is defined as dW/dh and one might expect, intuitively, that the stiffness will increase with decreasing film thickness and increasing pressure ratio. Figure 3.3 bears out this expectation except at the lower values of h_o , viz. $h_o < 20$ μm, where the stiffness dW/dh is seen to decrease with decreasing film thickness.

The curves of fig. 3.4 can be represented by the single empirical equation

$$W = \frac{180\ (P_s/P_a) - 150}{1 + 4.21 \times 10^{-4}\ (P_s/P_a)^{0.413}\ h_o^2} \qquad (3.1)$$

where, W is the load in newton

P_s is the absolute supply pressure

P_a is the atmospheric pressure

and h_o is the film thickness in μm.

It should be noted, however, that eq. 3.1 does not fit the curves for small film thicknesses as the equation predicts zero slope at $h_o = 0$ whereas the actual slopes of the $W - h_o$ curve are not zero at $h_o = 0$. At $h_o = 0$, of course, the stiffness has no meaning.

The bearing stiffness calculated by eq. 3.1 is plotted against the film thickness h_o in fig. 3.5 for different pressure ratios. The foregoing heuristic argument about the effect of the pocket stiffness can be extended a little further. For given pocket dimensions, the stiffness of the pocket will depend on the pocket

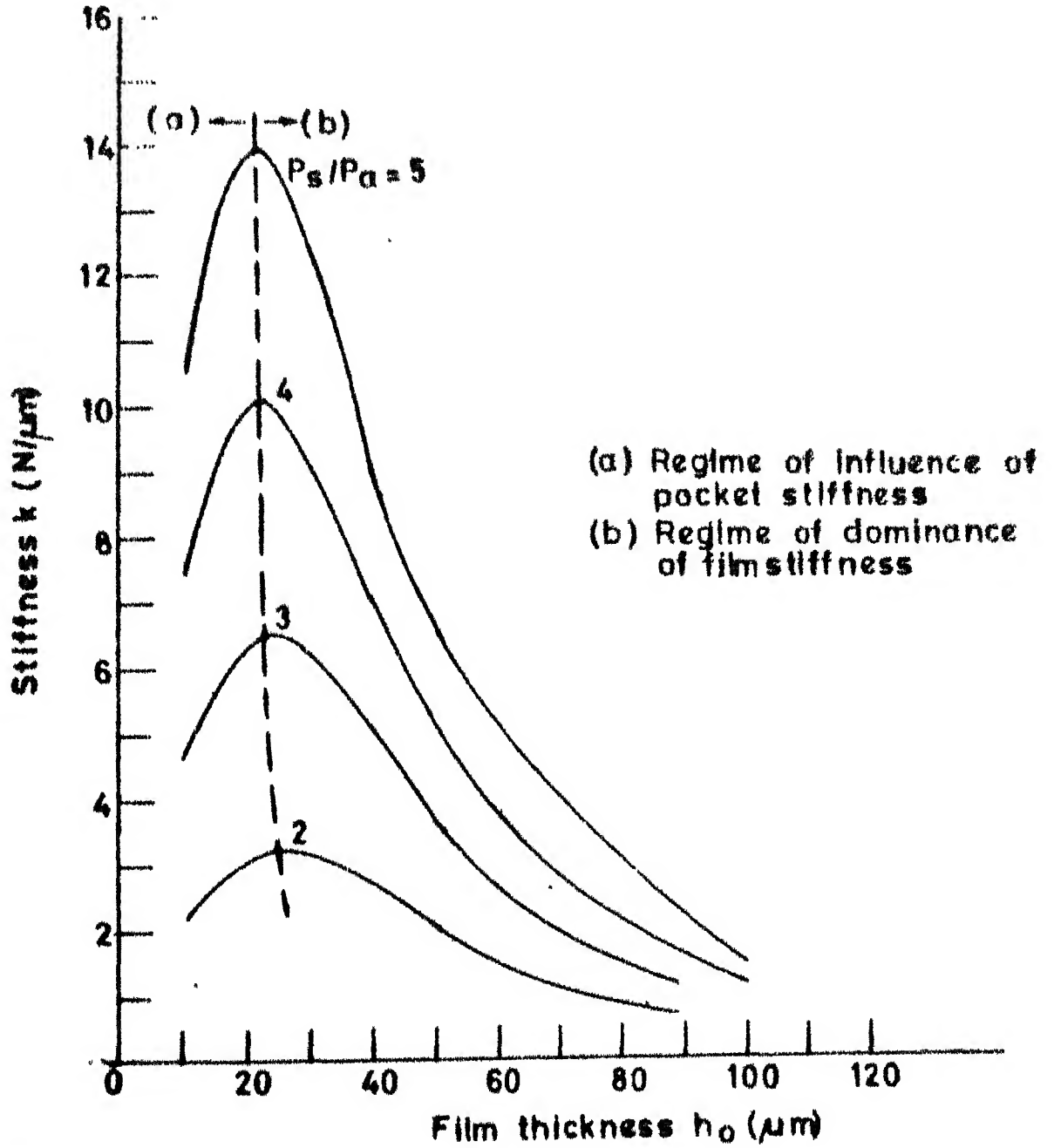

FIG. 3.5 GRAPH OF STIFFNESS Vs. FILM THICKNESS FROM EQUATION 3.1

pressure which, for unsteady loads, depends, in turn, on the supply pressure, the volume flow rate and the orifice dimensions. For given orifice dimensions and film thickness h_o , the flow rate is determined by the supply pressure (through (P_s-P_f)) and the higher this pressure, the higher will be the pocket stiffness. Thus, even in the regime of influence of the pocket stiffness (regime (a) in fig. 3.5) one expects that a larger pressure ratio will lead to a larger stiffness. Further, as the pressure ratio increases, one expects that the influence of the pocket stiffness will be felt at smaller values of h_o. Finally, since the pocket stiffness itself is larger at larger pressure ratios, one expects that the stiffness loss over some range of h_o , expressed as a fraction of the maximum stiffness, will be less for the larger pressure ratio. These arguments are supported by fig. (3.5).

Equation (3.1) can be used, in principle, to maximise the stiffness if maximum stiffness is the overriding concern in designing a bearing.

Figure (3.6) shows the variation of stiffness with pressure ratio for different values of h_o. For the present bearing, as already observed, the maximum stiffness corresponds to $h_o \simeq 20$ μm. If a desired value of stiffness is to be satisried, $h_o \simeq 20$ μm will also give

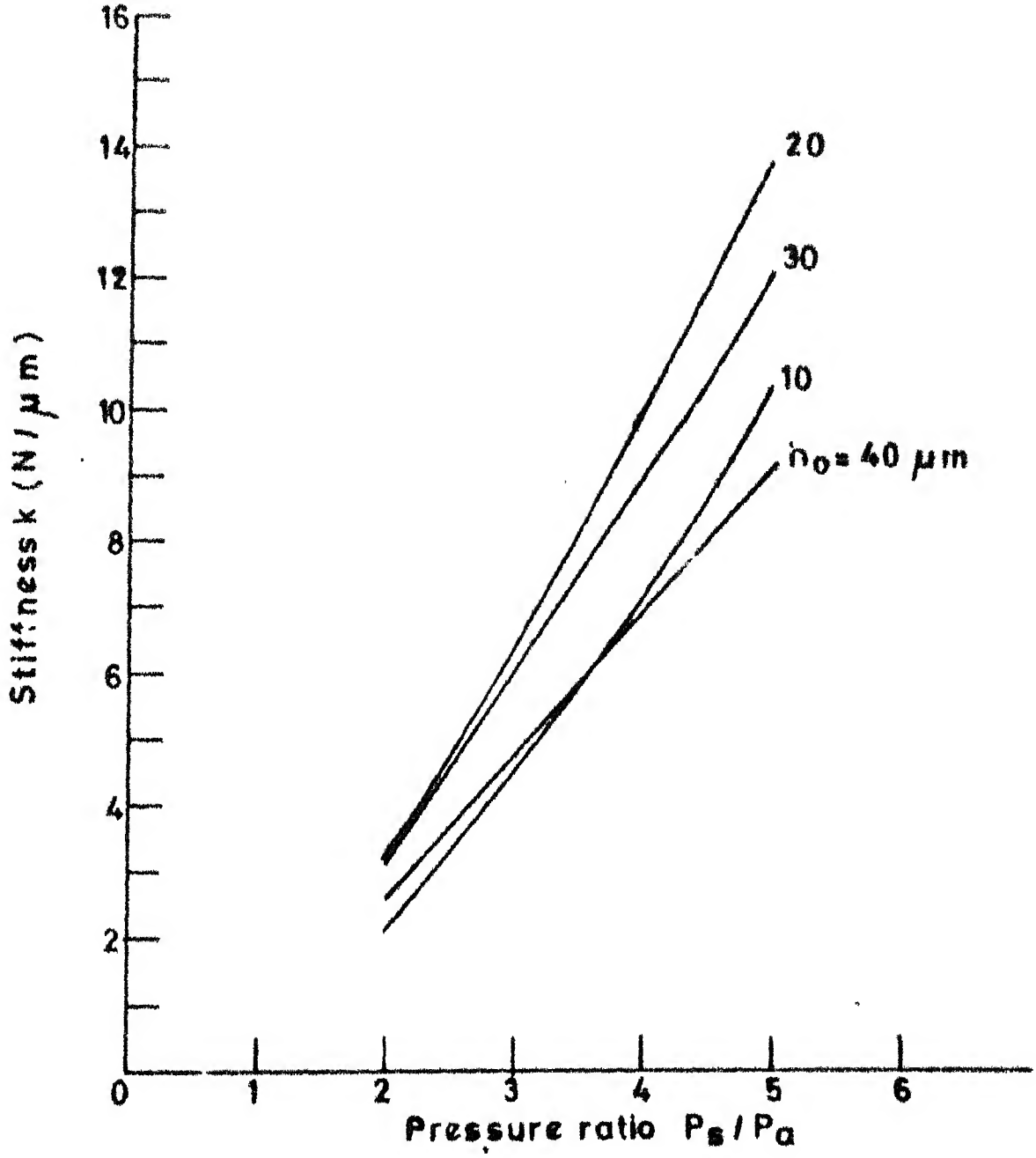

FIG. 3.6 GRAPH OF STIFFNESS Vs. PRESSURE RATIO FROM EQUATION 3.1

the smallest supply pressure. The lower the supply pressure, the smaller will be the compressor work.

3.4 Friction Test

Crude tests were made to determine the qualitative features of the dependence of frictional torque on air film thickness. In these tests, the shaft was spun by hand with different settings of the supply pressure regulator. The rotational speed of the shaft was determined by a stroboscope.

In accordance with the data of the tests described in article 3.2, a film thickness was assumed to correspond to each value of the supply pressure. The shaft was allowed to decelerate between two chosen values of rotational speed and the time of deceleration was measured by a stop watch reading to the nearest tenth of a second. This time average deceleration was assumed to be indicative of the frictional torque. The calculations are given in appendix II.

These tests were done with only one value of the load, viz. the dead weight of the shaft. Extra loads could not be applied because the loading arrangement, designed only for static tests, would have introduced very large frictional torques.

The results of this test is shown in Table 3.1. Figures 3.7 and 3.8 show the variation of frictional torque and the coefficient of friction, respectively, with the film thickness.

TABLE 3.1 : Results of friction test

Reading No.	Supply pressure (psig)	Δt (secs)	RPM_{start}	RPM_{end}
1	2	30.9	450	430
		38	300	280
		60	170	150
2	2.5	26.5	595	570
		24.5	450	430
		32.5	300	280
		46.5	170	150
3	5	21	595	570
		21.4	450	430
		28.2	300	280
		32.6	170	150
4	7.5	15.8	650	630
		21	595	570
		19.7	450	430
		25.4	300	280
		33.7	170	150
5	10	16.4	650	630
		21.9	595	570
		20	450	430
		26	300	280
		33.6	170	150

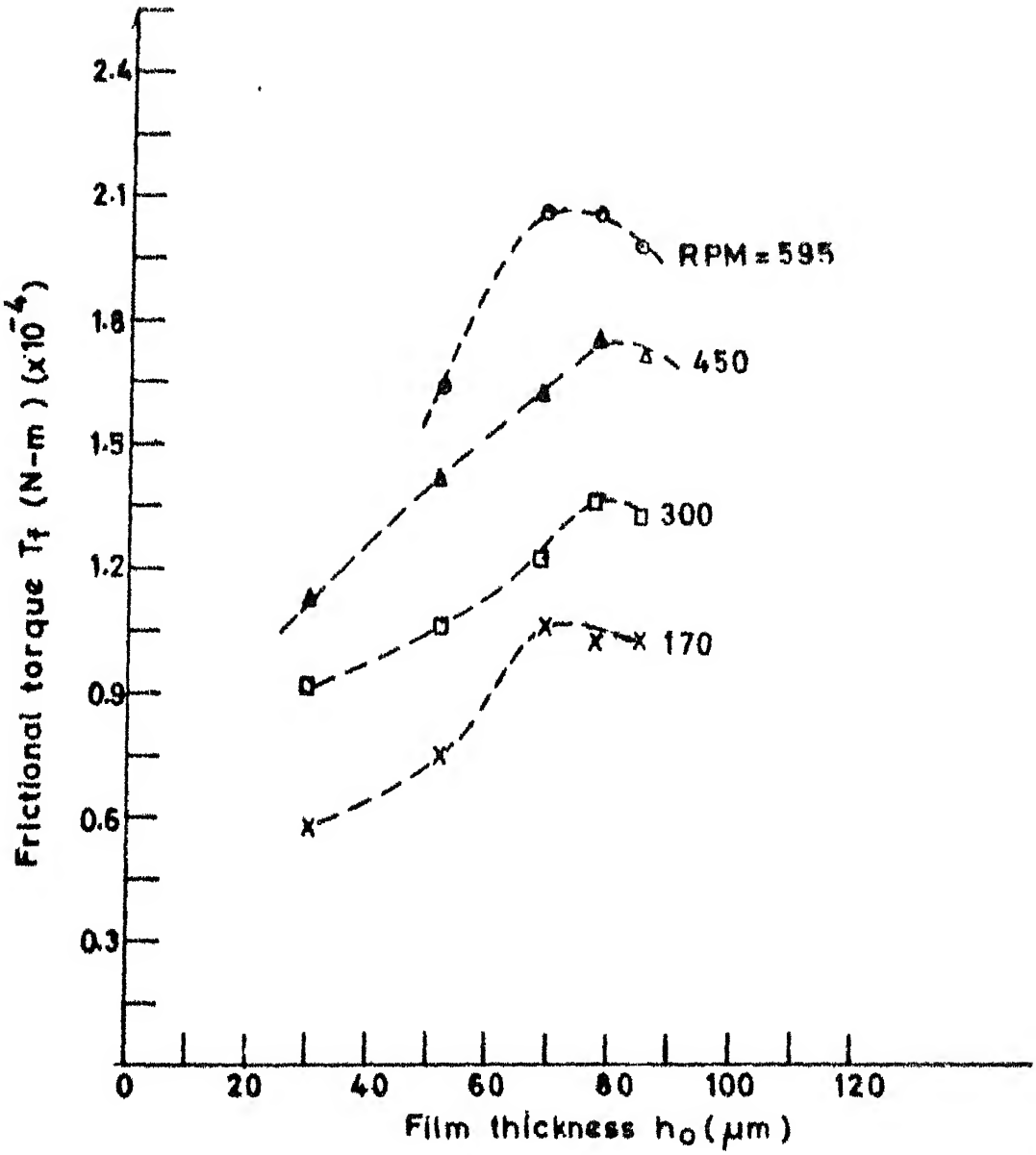

FIG. 3.7 GRAPH OF FRICTIONAL TORQUE Vs. FILM THICKNESS AT DIFFERENT RPMS.

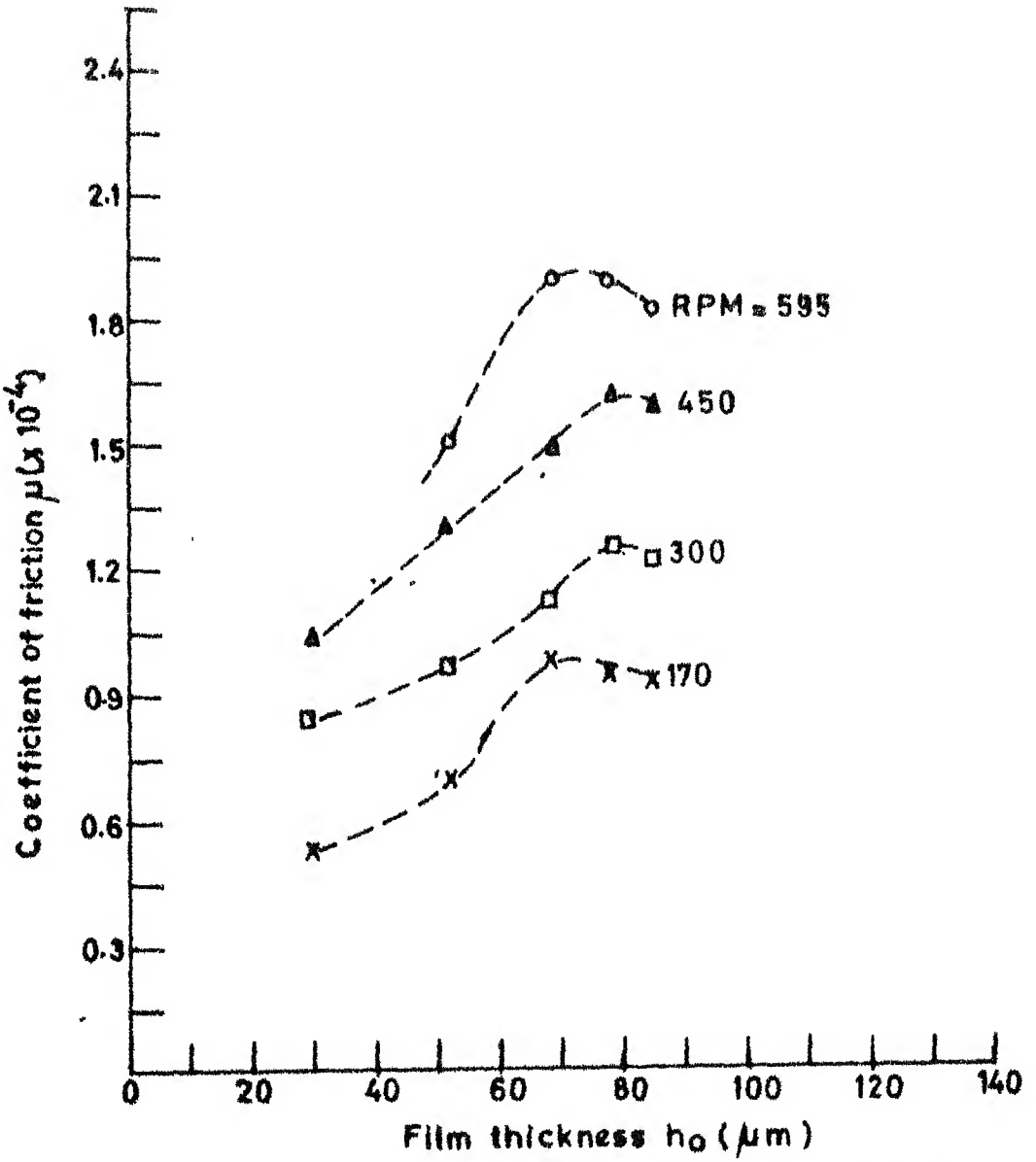

FIG.3.8 GRAPH OF EFFECTIVE COEFFICIENT OF FRICTION Vs. FILM THICKNESS AT DIFFERENT RPMS. THE EFFECTIVE μ IS EXCEEDINGLY SMALL OVER THE ENTIRE TEST RANGE

CHAPTER - 4

A SIMPLE DESIGN PROCEDURE

4.1 Introduction

In a given application, the shaft diameter and the load are known. The radial clearance c is based on the practicalities of machining. The bearing length L is often limited by the available space; if not , the L/D ratio is chosen in the neighbourhood of unity. Higher values of L/D lead to more serious problems with alignment, although the load capacity is improved. Smaller L/D ratios give a poorer load capacity. Frictional resistance in the bearing should, of course, be as low as possible but this is not of very great concern because it is inherently very small in aerostatic bearings. For certain applications, the bearing stiffness may be a crucial factor, in which case the design may be based on the maximum stiffness condition. In other cases, the frictional resistance and bearing stiffness may be simultaneously optimised. The most obvious optimisation would seem to be the one where the energy requirement is minimised by optimising

the compressor work and the frictional dissipation. The present experimental data indicate that, for partial journal bearings, the compressor work and frictional loss are simultaneously minimised by minimising the film thickness h_o (friction data were taken only for $h_o \geq 30$ μm). The minimum film thickness is limited by the quality of the surface finish.

With the above in mind, the task of designing an aerostatic partial journal bearing consists of determining the dimensions and disposition of the orifices and the pockets and also the operating supply pressure commensurate with such others requirements as stiffness. In the following sections is presented a simple approach to the design which does not include consideration of maximum stiffness requirements (aerostatic bearings, inherently, have high stiffness in the operating regime recommended here) nor quantifies the pocket dimensions. The effects of the pocket dimensions, however, are briefly commented upon.

4.2 The Rationale

The graph of film thickness versus supply pressure (fig. 3.3) shows that h_o decreases with decreasing P_s when the load W is a constant. It has been observed in article 3.3 that, with constant W, the

volume flow rate also decreases with decreasing P_s. Thus the compressor work is minimised by minimising P_s.(For bearing applications, the reciprocating compressor with a reservoir is the natural choice).

The relationship between the supply pressure P_s and the load W, for constant h_o , is fairly complicated. The average film pressure P_f , however, is a linear function of the load:

$$P_f = \frac{W}{LD} \qquad (4.1)$$

This suggests a means of relating P_s with W. If P_s is comparable to P_f, P_s may be assumed to have a linear relationship with W. Since the orifice pressure drop $(P_s - P_f)$ increases with increasing flow rate, the pressures P_s and P_f are comparable when the flow rate is very small. This can happen under two conditions:

i) When the load is very light. In that event, even a nominal supply pressure $P_s > P_a$ may result in a large film thickness h_o but the flow rate remains small.

ii) When the load is very large. In this case the flow rate and hence the pressure drop $(P_s - P_f)$ can be small only if the film thickness is very small.

On the basis of the above argument, one might conclude that, with h_o as a parameter, W and P_s can be

linearly related (approximately) if the supply pressure is very small or if the load is very large. These expectations are represented in fig. 4.1 and confirmed by fig. 4.2 which shows the present results.

Thus, it seems logical to assume a value for h_o commensurate with a small flow rate (small flow rates correspond to small compressor work) and then to estimate the required P_s from the linear equation approximately relating P_s and W. If one writes this relationship in the form

$$W = f(h_o)\, P_s + C$$

it is seen that dimensional consistency requires that

$$f(h_o) \propto h_o^2$$

Attempts to obtain such an empirical fit from fig. 4.2 proved difficult. It was realised, further, that the built-in-radial clearance c must also affect the performance of the bearing. Subsequently, the parameter h_o was replaced by $\alpha = h_o/c$.

The dimensionless quantity α is akin to the eccentricity ratio (ε) usually defined for full journal bearings. The eccentricity ratio, however, is an inconvenient parameter for aerostatic partial journal bearings in which the film thickness is determined by

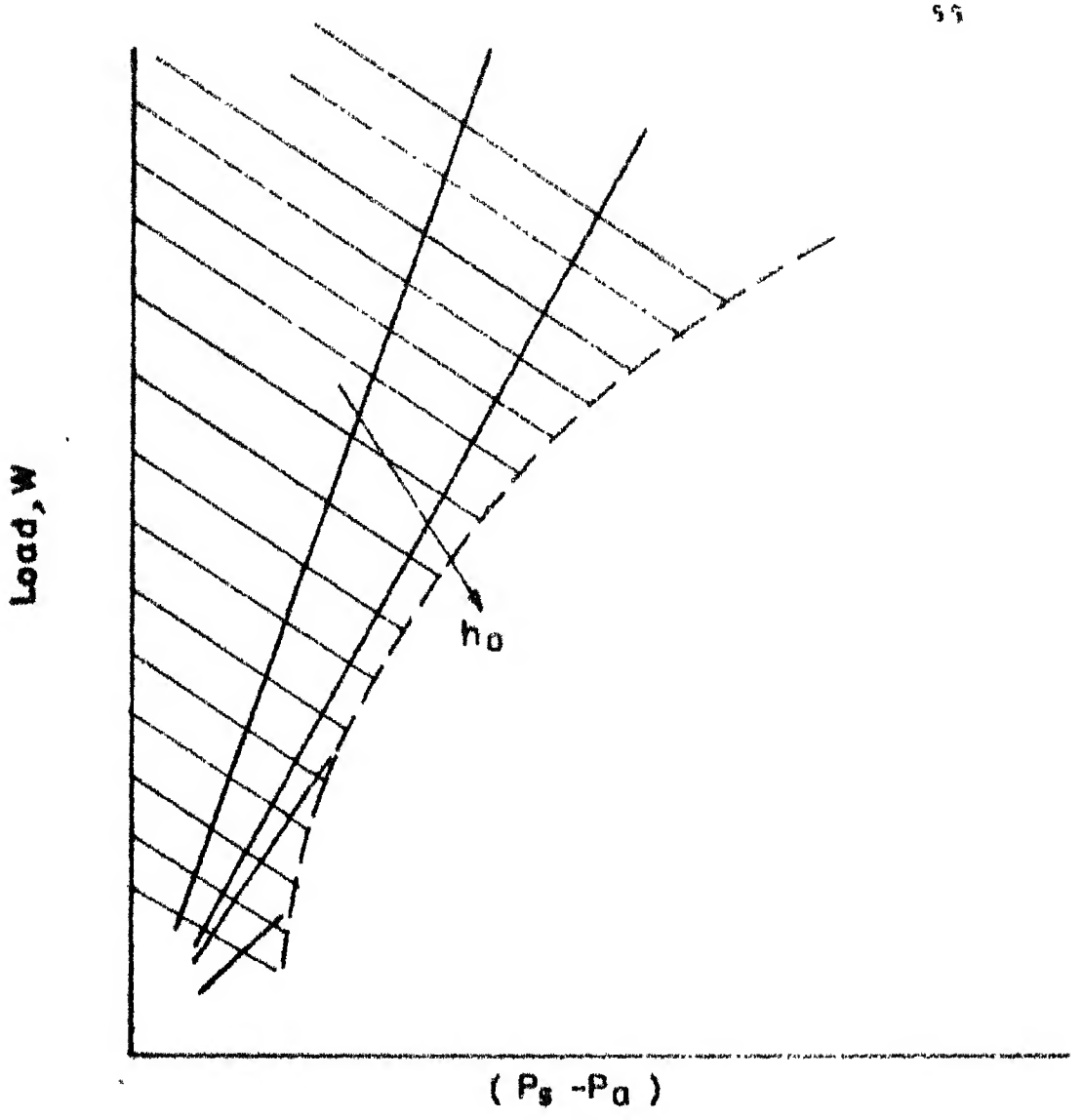

FIG. 4.1 THE DOMAIN OF THE EXPECTED LINEAR RELATION-SHIP BETWEEN LOAD AND SUPPLY PRESSURE (For large h_0, the approximate linearity holds only for small P_s; for small h_0, it holds upto large P_s)

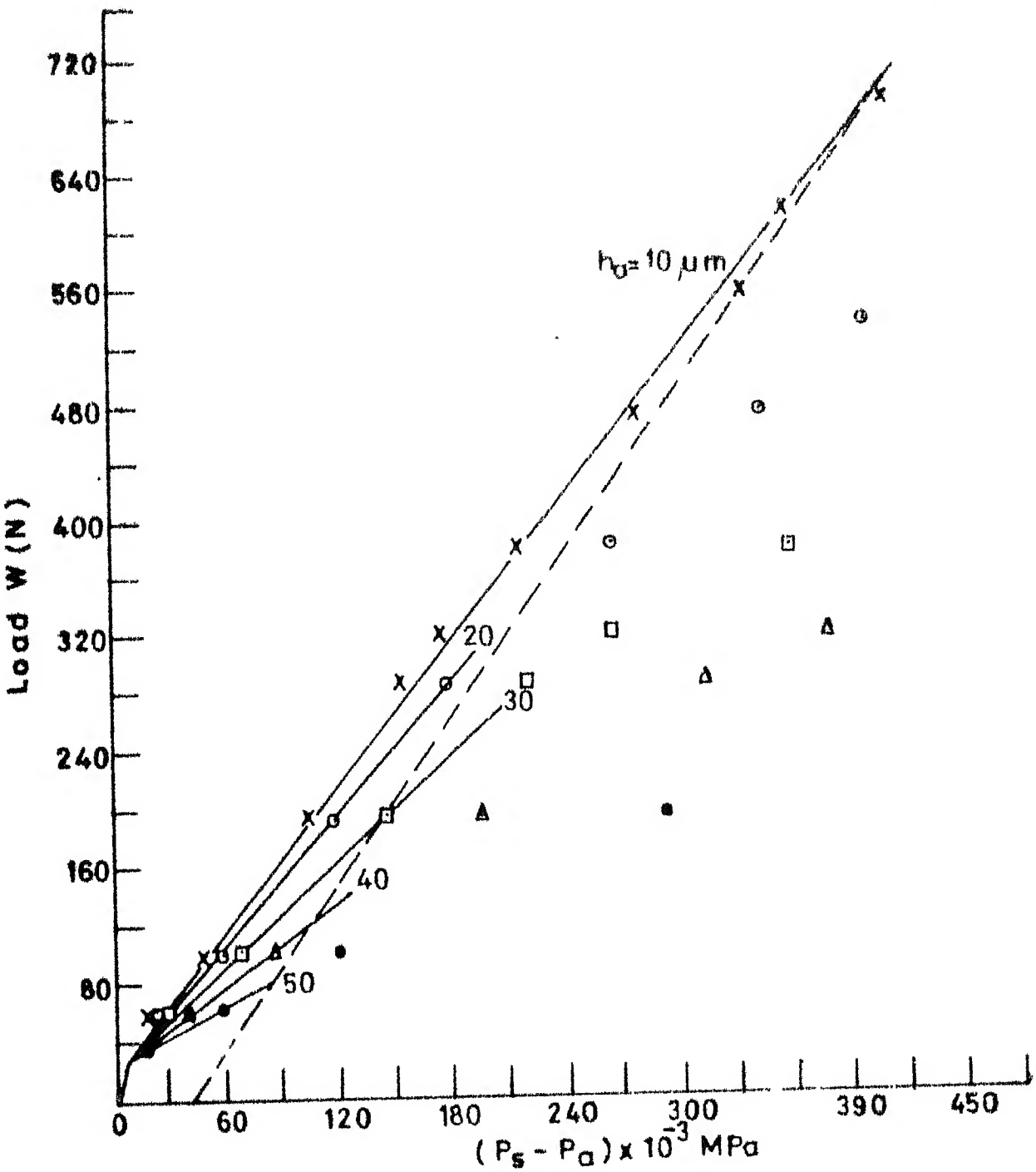

FIG. 4.2 GRAPH OF LOAD Vs. SUPPLY PRESSURE
(Data points are taken from the curves of fig 3.3)

the supply pressure and it is possible to have $h_o > c$, in which case the eccentricity and hence ε become negative. The quantity α, as defined here, can be greater or less than unity.

The advantage of introducing α into the equation relating P_s to W is that, all powers of α are admissible from the viewpoint of dimensional consistancy. Thus, one can postulate

$$W = f(\alpha)\ P_s(LD) + C \qquad (4.2)$$

where $f(\alpha)$ may be written as a power series and a fit can be sought between eq. 4.2 and the graphs of fig. 4.2. Thus,

$$f(\alpha) = a_1 + b_1\alpha + c_1\alpha^2 + \ldots\ldots \qquad (4.3)$$

in which the number of terms (and hence the number of unknown coefficients) depends on the accuracy desired. Since the present data provide only five values of α (fig. 4.2) at most five terms can be admitted. The approximate nature of the model, however, may not justify such accuracy in the determination of $f(\alpha)$ and only three terms have been used.

Figure 4.2 seems to indicate a common intersection point for the straight lines of different h_o values. Below this intersection, all the constant h_o

lines seem to merge and proceed to the origin of the plot and the linear relation between W and P_s becomes independent of h_o. In fact, of course, there is no unique intersection point; the constant h_o lines bend and proceed smoothly to the origin. The empirical relation given below (eq. 4.4) holds for the straight lines above the so-called intersection point.

Combining eqs. (4.2) and (4.3) and substituting data from the curves for h_o equals to 10 μm, 20 μm and 30 μm (i.e., within the range of reasonable h_o) the following empirical relation is obtained:

$$W = [0.49-0.02\alpha-0.24\alpha^2] (P_s-0.107) LD + 28 \quad \ldots \quad (4.4)$$

in which P_s is the absolute supply pressure in MPa and the constant 28 is in newton. The term in parentheses stands for the measured (gauge) supply pressure.

4.3 Design Procedure

As outlined in article 4.1, one starts with a given load, bearing length and diameter, and an assumed radial clearance c. One then chooses a small but realistic value of h_o , so as to have a realistic α.

With the above values, one goes to eq. 4.4 to estimate the supply pressure P_s. This is applicable

for two rows of orifices as in the present bearing. If the number of rows is increased, the required supply pressure is expected to be a little lower. Two rows, of course, is the optimal choice in that the cost of the bearing will be minimised while retaining stiffness against shaft tilt. For low L/D ratios, a single row may suffice and the stiffness against shaft tilt is then provided by the two bearings in conjunction. The present model, however, may become too inaccurate for the single row case.

The orifice diameter will depend on the flow rate. The mass flow rate of air through an orifice is given by [12]

$$m = C_D A \rho_s (2RT_s)^{1/2}\left[\frac{\gamma}{\gamma-1} \left\{ (P_2/P_1)^{2/\gamma} - (P_2/P_1)^{\frac{\gamma+1}{\gamma}} \right\} \right]^{1/2} \quad \ldots\ldots \quad (4.5)$$

where isentropic expansion has been assumed. The symbols in eq. 4.5 are explained in the nomenclature. The downstream pressure P_2 (pocket pressure) can be calculated approximately in terms of P_f assuming the axial flow model of fig. 1.1.

$$P_2 = P_f \left(\frac{L}{L-1} \right) \quad \ldots \quad (4.6)$$

The upstream pressure P_1 is, of course, the supply pressure P_s. To obtain P_f , use is made of eq. 4.1.

The total mass flow rate for the bearing has to be assumed, the idea being to have as small a flow rate as possible (In the present bearing, for example, the mass flow rate was estimated to be 2.5×10^{-3} kg/s). It is possible, in principle, to estimate the total mass flow rate by invoking the pressure distribution model of fig. 1.1, but this approach is not shown here. Instead, it is suggested that a flow rate M be assumed and the orifice area A be determined for this value of M ; the exercise can then be repeated until a realistic orifice diameter is obtained. Conversely, one can start with a chosen orifice diameter and estimate m and hence $M = m N_T$ and then estimate the corresponding compressor power.

Before one can perform the exercise outlined in the preceding paragraph, one has to choose the number of orifices per row. The minimum number, quite clearly, is three for a partial aerostatic journal bearing. The greater this number, the more uniform will be the radial stiffness all around the bearing. On the other hand, too large a number will lead to an unnecessarily large flow rate since P_f and P_s have been fixed already. In the present procedure, three to five orifices per row are recommended. (It is expected that the approximate number of orifices per row will depend on the

radius of the bearing, but this has not been proved here. In the present bearing , $\frac{D}{n} \simeq 12$ mm and this is recommended as a guide to the selection of the number of orifices per row).

Once the number of orifices per row and the number of rows is chosen, eq. 4.5 gives the orifice area for the assumed $m = \frac{M}{N_T}$. This gives the orifice diameter d_o.

Example

Problem: An externally pressurized half journal bearing is to be designed to carry a load of 100 N. Compressed air is available at $\frac{P_s}{P_a} = 4$. The airflow should not exceed 10^{-4} m^3/s. The shaft diameter is 32 mm but there is no restriction on the bearing length.

Using eq. 4.4, we can find the absolute supply pressure P_s for a load of 100 N.

We shall choose $\alpha = 0.5$ which, for a radial clearance $c = 20$ μm, gives a film thickness $h_o = 10$ μm, and $\frac{L}{D} = 1$ (i.e. L = 32 mm)

We get, $P_s = 274.71 \times 10^{-3}$ MPa which corresponds to $\frac{P_s}{P_a} = 2.7$ So, the supply pressure is acceptable.

Using eq. 4.1, we find the average pressure in the film,

$$P_f = \frac{100}{32 \times 32} = 97.66 \times 10^{-3} \text{ MPa (gauge)}$$

$$\therefore \quad P_2 = \left(\frac{L}{L-1} \right) P_f = 231.51 \times 10^{-3} \text{ MPa}$$

$$\therefore \quad \frac{P_2}{P_1} = 0.84$$

The density of air at atmospheric pressure and 20°c

$$= 1.201 \text{ kg/m}^3.$$

From the perfect gas law, and assuming a room temperature of 20°c

$$\rho_s = \left(\frac{P_s}{P_a} \right) \rho_a \quad ; \quad \text{where } P_a \text{ and } \rho_a \text{ are atmospheric values.}$$

$$= 3.257 \text{ kg/m}^3$$

$R = 287$ J/kg °K

$T_s = 293$°K

$C_D = 0.8$ (standard value, ref. [12])

$\gamma = 1.4$

$M = 10^{-4}$ kg/s

Equation 4.5 gives, for 3 orifices per row (because $\frac{D}{n} \simeq 12$ gives $n \simeq 3$) and using 2 rows,

$$d_o = 0.23 \text{ mm}.$$

4.4 Design of Pockets

The present procedure does not include the means of quantifying the pocket dimensions. The pocket

diameter is limited by the bearing length and diameter and also by the number of orifices. Further, the pocket volume influences the bearing stiffness, as discussed in article 3.3. Also, the pocket dimensions have a marked effect on the likelihood of instabilities. Stout et al [11] recommend that the ratio of the radial clearance volume to the total pocket volume should be of the order of 20 for full journal bearings. The higher this ratio, the less will be the likelihood of occurrence of instabilities. In the present partial journal bearing, this ratio is about 9.5 but, in this context, the radial clearance is not the appropriate parameter to use for a partial bearing.

Stout et al [11] also recommended that the pocket diameter should be chosen with

$$d_R \geq \frac{d_o^2}{2c}$$

for full journal bearings. In view of our earlier argument that the film thickness is more appropriate than the radial clearance, for partial journal bearings, we write Stout's criterion as

$$d_R \geq \frac{d_o^2}{2h_o}$$

Then, for the bearing designed in the example of article 4.3, with $d_o = 0.23$ mm and $h_o = 10$ μm (i.e. $c = 20$ μm),

we have

$$d_R \geq 2.64 \text{ mm.}$$

Following Stout's recommendation for pocket volume, with h_o again replacing c, we have total pocket volume $\simeq 0.804 \text{ mm}^3$ so that for six pockets, the depth of each pocket is

$$h_R \simeq 25 \ \mu\text{m}$$

It is to be noted that, by using h_o in place of c, h_R has been underestimated. This pocket depth is too small from the point of view of the convenience of machining. If we increase the operating film thickness to $h_o = 20 \ \mu\text{m}$ (while retaining $\alpha = 0.5$), we shall need a radial clearance of $c = 40 \ \mu\text{m}$ and then, with $d_R \simeq 1.3$ mm., the recommended pocket depth is $h_R \simeq 101 \ \mu\text{m}$. This new set of values is better in that machining requirements have become less demanding without affecting the mass flow rate.

4.5 Comments

The design procedure outlined in the present chapter applies only to partial journal bearings. The operational characteristics of a full journal bearing are different. Thus the load capacity, frictional torque and stiffness of a full journal bearing cannot

be determined by a simple extension of the results for a partial journal bearing. One final word of caution: the present design approach applies only within the regime of validity of the linear model as indicated in fig. 4.2, but this regime has not been categorically defined for want of an adequate body of data. The present data are from tests performed on a single bearing. It is assumed that the results presented in this chapter are valid for all bearings of similar type and size; the worth of the design procedure can be evaluated only after bearings designed by this method are tested for performance.

CHAPTER - 5

CONCLUDING REMARKS

When the direction of the load is steady, partial journal bearings are effective. They possess the advantage of having less frictional resistance than full journal bearings. Their characteristics, however, are qualitatively different from those of full journal bearings.

In the present work, an aerostatic half journal bearing has been designed on the basis of the design charts of Stout et al [11]. These charts are for full journal bearings, but proved to be successfully applicable to the present half bearing as well. A modification of Stout's recommendations is necessary in order to avoid instabilities, but this has not been done while designing the bearing. It has, however, been discussed in the presentation of a new design procedure given in Chapter 4.

The main objective of the work was to design and build a successful bearing. This objective has been achieved and the performance of the bearing has

been partially tested.

Some interesting results have emerged from the test data. The stiffness of the bearing is seen to increase with decreasing film thickness until the film thickness becomes so small that the stiffness of the pocket becomes predominant. From that point, the stiffness falls with decreasing film thickness. The frictional torque on the shaft is seen to increase with increasing film thickness. This is contrary to expectation and no explanation has been found for it.

A simple design procedure, based on the results of the tests, has been formulated. Though somewhat limited in scope, this procedure, which uses simple algebraic relations, has the advantage of providing some insight into the physics of operation of aerostatic partial journal bearings, thus enabling the designer to visualise the effects of changing the design parameters. It answers the most common need of the designer, viz. to determine the required supply pressure when the load and overall bearing dimensions are given a priori. The supply pressure is estimated from a simple empirical equation (eq. 4.4) in which the non-dimensional film thickness α is used as a chosen input. Once the supply pressure is determined the actual film thickness in

operation will depend on the initial radial clearance c. The orifice diameter is then determined on the basis of a desired flow rate (eq. 4.5).

The tests were rather limited in scope and so the results presented in Chapter 4 should be considered to be tentative.

Recommendations for Future Work

The present work can be extended to do the following:

i) The present set up is unsatisfactory. A more permanent arrangement has to be done for further experimentation.

ii) The bearing performance should be studied, while the journal is in rotation.

iii) Friction tests should be carried out for smaller film thicknesses.

REFERENCES

1. Laub, J.H., "Hydrostatic gas bearings", Trans. ASME, Series D, Vol. 82, 1960, pp. 276-286.

2. Cameron, A., "Hydrostatic bearings", Basic Lubrication Theory, Chap. 12, John Wiley and Sons, 1976, pp. 142-144.

3. Shires, G.L., " The design of externally pressurized bearings", Gas Lubricated Bearings, Grassam, N.S., and Powell, J.W., eds., Butterworths, 1964, pp. 110-139.

4. Robinson, C.H., and Sterry, F., " The static strength of pressure fed gas journal bearings", A.E.R.E. Rep. R/R 2642, Sept. 1958.

5. Shires, G.L., " Experiments with an air lubricated journal bearing", National Gas Turbine Establishment Memo No. M 49, May 1949.

6. Pinkus, O., and Sternlicht, B., "Hydrodynamic gas bearings", Chap. 5, New York; McGraw-Hill, 1961.

7. Shires, G.L., " The vented pressure-fed gas journal bearing" U.K.A.E.A., Winfrith, AEEW-R111, March 1962.

8. Lemon, J.R., " Analytical and experimental study of externally pressurized air lubricated journal bearings", Trans. ASME, Series D, Vol. 84, No. 1, Mar. 1962, pp .159-165.

9. Powell, J.W., Moye, M.H., and Dwight, P.R., " Fundamental theory and experiments on hydrostatic air bearings", Instn. Mech. Engrs, Lubrication and Wear Convention, Bournemouth, May 1963.

10. Mazumder, B.C., " On the general solution of externally pressurized gas journal bearings", Trans. ASME, Series F, Vol. 94, No. 4, Oct. 1972, pp . 291-296.

11. Stout, K.J., Tawfik, M., and Pink, E.G., " Design of externally pressurised fluid-film bearings - Design of aerostatic journal bearings", Engineering (London), Vol. 219, No. 2, Feb. 1979, pp . 143-147.

12. Powell, J.W., " Theory of aerostatic lubrication", Design of Aerostatic Bearings, Chap. 2, The Machinery Publishing Co. Ltd., 1970, pp . 42-43.

APPENDIX - I

SPECIFICATIONS OF SOME OF THE ELEMENTS USED IN THE EXPERIMENTAL SET UP

i) Air compressor : ELGI Equipments Pvt. Ltd., (India)

Displ. Vol - 1555 litre/min

Working pr. - 12 atu

Motor - 15 hp

RPM - 1150

Tank capacity - 750 litre

ii) Pressure regulator : United States Gauge

Range 0 - 100 psi

Resolution - 2.5 psi upto 10 psi

2 psi above 10 psi

iii) Dial indicator : Rambold (Germany)

Range - 0.001 mm - 2 mm

Resolution - 1 μm

iv) Stroboscope : General Radio Company Concord Massachusetts, USA.

Range - 110 - 25000 rpm

v) Stop watch : Racer (Swiss made)

Range - $\frac{1}{10}$ s - 15 min

Resolution - 0.1 s

APPENDIX - II

CALCULATIONS OF FRICTIONAL TORQUE AND COEFFICIENT OF FRICTION

Frictional Torque Calculation

Average angular acceleration $= \frac{\omega_1 - \omega_2}{\Delta t}$

$$= \frac{2\pi\ (RPM_{start} - RPM_{end})}{\Delta t \times 60}$$

$$\text{rad/sec}^2$$

Where, ω_1 and ω_2 are angular velocities and Δt is the time interval in seconds.

Frictional torque,

T_f = (mass moment of inertia of the shaft) x angular acceleration

$= \frac{\text{mass} \times (\text{radius})^2}{2} \times$ angular acceleration

Effective coefficient of friction calculation

$$T_f = F \times \frac{D}{2}$$

where, F = effective friction force

Again, $F = \mu N$

where, μ is the coefficient of friction and the average normal reaction N is equal to the shaft load W

$\therefore \quad T_f = \mu N \times \frac{D}{2}$

or, $$\mu = \frac{T_f \times 2}{D \times N}$$

These calculations lead to the results shown in figs. (3.7) and (3.8).

APPENDIX-III

FURTHER INVESTIGATION OF THE FRICTIONAL TORQUE

As stated on page 67, the increase of the frictional torque with increasing film thickness could not be explained. As this thesis was being submitted, it was realised that the friction tests had been done for only one direction of rotation of the shaft. When additional tests were done, after carefully aligning the rig, it was found that the frictional torque was strongly dependent upon the direction of rotation! Moreover, the results of fig. 3.7 and 3.8 could not be reproduced.

It was inferred that asymmetries of the rig were responsible for the observed effect. Asymmetry could be a consequence of a small residual misalignment, or it could be a result of imperfections in the fabrication of the rig. Errors of the order of only a few microns are involved, and with the measuring equipment available it was not possible to identify the source of the asymmetry.

It is believed that asymmetry results in the circumferential flows on the two sides of the plane of symmetry being dissimilar, even with the shaft at rest. Consequently, the skin friction acting on the shaft

is unbalanced and gives rise to a net torque. As a result, the measured frictional torque changes when the direction of rotation is changed.

In view of the foregoing, it is felt that measurements of the coefficient of friction should be performed only after a more precise experimental rig is available.

It is emphasized that the stiffness measurements reported here are reliable and the results of these measurements were repeatable.